



**HAL**  
open science

## A model for the influence of work hardening and microstructure on the evolution of residual stresses under thermal loading – Application to Inconel 718

J.P. Goulmy, L. Toualbi, V. Boyer, P. Kanoute, D. Restraint, E. Rouhaud

### ► To cite this version:

J.P. Goulmy, L. Toualbi, V. Boyer, P. Kanoute, D. Restraint, et al.. A model for the influence of work hardening and microstructure on the evolution of residual stresses under thermal loading – Application to Inconel 718. *European Journal of Mechanics - A/Solids*, 2024, 107, pp.105361. 10.1016/j.euromechsol.2024.105361 . hal-04634663

**HAL Id: hal-04634663**

**<https://hal.science/hal-04634663>**

Submitted on 4 Jul 2024

**HAL** is a multi-disciplinary open access archive for the deposit and dissemination of scientific research documents, whether they are published or not. The documents may come from teaching and research institutions in France or abroad, or from public or private research centers.

L'archive ouverte pluridisciplinaire **HAL**, est destinée au dépôt et à la diffusion de documents scientifiques de niveau recherche, publiés ou non, émanant des établissements d'enseignement et de recherche français ou étrangers, des laboratoires publics ou privés.



## 31 Introduction

32 In order to improve the fatigue life of critical components, surface improvement methods such as shot  
33 peening are widely used in the aerospace industry. This process generates superficial compressive  
34 residual stresses that tend to delay fatigue crack initiation and prevent small crack propagation [1], [2],  
35 [3], [4], [5]. For structures that experience high temperature variations in service, these surface  
36 enhancement methods are only efficient if the thermo-mechanical relaxation of the generated residual  
37 stress field is moderate at operating temperatures. It is however observed that relaxation due to  
38 thermal effects is far from being negligible in high-temperature fatigue tests [6]. It is therefore  
39 important to understand the mechanisms that induce the thermal relaxation of residual stresses in  
40 order to further input these effects into a model. One of the critical points is to estimate the kinematic  
41 and time constants of this relaxation.

42 The nickel-based superalloy Inconel 718 is widely used in the aeronautical industry. In its standard  
43 metallurgical state known as Direct Aged (DA), this alloy features a microstructure with a  $\gamma$  matrix  
44 composed of grains of about 5  $\mu\text{m}$ ,  $\gamma'/\gamma''$  strengthening precipitates of a few nanometers, a  $\delta$  phase  
45 anchored at the grain boundaries, as well as carbides and nitrides that locally harden the matrix [7],  
46 [8], [9], [10]. Subjected to temperatures close to 550°C, Inconel 718 turbine discs undergo thermo-  
47 mechanical stresses in service. These discs can present microstructural heterogeneities because of  
48 their manufacturing process history; they can also undergo more than ten conditions of shot peening  
49 treatment, depending on their geometry. The in-service evolution of residual stresses in these parts  
50 can therefore be particularly diverse and complex. In order to evaluate the benefits of shot peening on  
51 the fatigue life of these parts, it is necessary to understand the microstructural changes induced by  
52 shot peening and their influence on the thermal relaxation of residual stresses. Inconel 718 thus  
53 constitutes a material of interest to study and model residual stress relaxation due to thermal loading.  
54 Clearly, microstructural parameters of Inconel 718 have a significant influence on the tensile, fatigue,  
55 and creep properties [7], [8], [9]. Furthermore, previous studies [11], [12] have highlighted the  
56 influence of microstructural modifications on the residual stress and work hardening profiles induced  
57 by shot peening. It was shown that work hardening is significantly affected by a change in grain size.  
58 On the contrary, changing the grain size or the size of the strengthening precipitates  $\gamma'/\gamma''$  appears to  
59 have minimal effect on the residual stress profile. It is then useful to define how these different profiles  
60 relax with time.

61 Many authors [13], [14], [15], [16], [17] have described the thermal relaxation of residual stresses  
62 caused by shot peening. By relaxation, it is here meant a lowering of the local absolute value of the  
63 residual stress level. The main observations are: (i) the higher the temperature, the higher the  
64 relaxation of the residual stresses combined with the fact that relaxation is negligible below a threshold

65 temperature, except at the surface where a change may occur depending on the shot peening  
66 condition used; (ii) relaxation is observed at each depth of the profile, hence, the general shape of the  
67 profiles (position of the maximum stress, position of the tensile transition) is not changed, except above  
68 a certain temperature where a shift from the top of the profile to the core of the part is observed (iii)  
69 for a given temperature, the main evolution of the residual stresses takes place during the first instants  
70 of temperature holding, then, the residual stress profiles tend to asymptotic profiles with time.

71 The impact of work hardening on the relaxation of residual stresses has also previously been  
72 characterized in the literature [6], [18], [19], [20], [21], [22]. Prev y observed that there is a threshold  
73 value (3% of work hardening) below which no relaxation of residual stresses is observed [6]. Above this  
74 threshold, many authors have shown that the greater the work hardening induced by shot peening,  
75 the greater the relaxation of residual stress [6], [18], [19], [21], [22]. These studies explain that residual  
76 stress relaxation is related to the density of dislocations in the material: the higher the number of  
77 dislocations, the more the residual stresses relax. It is in particular observed that the laser shock  
78 process, known to induce low work hardening levels, results in much lower residual stress relaxation  
79 than shot peening [6]. Prev y also established that residual stress relaxation is influenced by the level  
80 of work hardening and not the method of work hardening introduction.

81 The residual stress and work hardening profiles resulting from the different manufacturing processes  
82 used for industrial parts vary considerably. Consequently, controlling the relaxation of residual stresses  
83 has become challenging and requires the development of appropriate models. The most widely used  
84 model for the thermal relaxation of residual stresses is the Zener-Wert-Avrami model [16], [20], [23],  
85 [24], [25]. It predicts stress relaxation without taking work hardening into account. Its parameters are  
86 therefore only identified for a specific operating point (a microstructure, a position in a sample, a  
87 manufacturing process, and a temperature). Hoffmeister *et al.* proposed a more complex model to  
88 account for microstructural effects [16]. Here again, the model depends on a specific operating point  
89 and is not able to predict the relaxation of residual stresses in depth unless a large set of measurements  
90 is available to identify a set of parameters for each test condition. Thus, although the influence of work  
91 hardening on the relaxation of residual stresses has been clearly established through several  
92 experimental observations, to date, there is no model available in the literature taking these effects  
93 into account. It should also be noted that the influence of the microstructure and its relationship to the  
94 effect of work hardening is relatively rarely, if ever, discussed in the literature.

95 The purpose of this paper is to investigate the impact of work hardening and microstructure on the  
96 thermal relaxation of residual stresses caused by shot peening on Inconel 718. The main objective is to  
97 propose a model that accurately accounts for these effects. This paper is composed of three sections.  
98 The first section describes the experimental methods starting with the description of the reference  
99 material microstructure of Inconel 718. In addition, this section presents the different thermal

100 treatments proposed to obtain two complementary microstructures, as well as shot peening conditions  
101 and procedures to characterize residual stresses and work hardening. The second section presents and  
102 compares the results obtained after shot peening and after thermal relaxation at 550°C of shot peened  
103 parts. The influence of work hardening and microstructure on the relaxation of residual stresses is  
104 discussed. The final section describes the proposed model for thermal relaxation of residual stresses  
105 accounting for the influence of work hardening. The developed analytical model is validated on a large  
106 set of data using complementary results from the literature.

## 107 **1 Materials and methods**

### 108 **1.1 Inconel 718**

109 The investigated material is Inconel 718 with a  $\gamma$  matrix; its composition is given in Table 1. The  
110 influence of the microstructure is evaluated through the study of three different microstructures. First,  
111 the *reference* microstructure, obtained after manufacturing and corresponding to the “as-received”  
112 material, known as Direct Aged (*DA*). The other two microstructures, namely coarse grain  
113 microstructure (*CG*) and coarse grain and coarse strengthening precipitates microstructure (*CGCP*),  
114 exhibit parameters that have been modified by means of a specific heat treatment history. The  
115 microstructure of *CG* was achieved by annealing at 1040°C for 30 minutes, followed by  $\delta$  phase  
116 precipitation treatment at 955°C for one hour, and finally by conventional  $\gamma'/\gamma''$  strengthening  
117 precipitation treatment (8 hours at 720°C followed by cooling at 50°C/h and aging at 620°C for 8 hours).  
118 The *CGCP* microstructure is characterized by coarse grains and large strengthening precipitates. The  
119 heat treatment sequence applied to the *CG* microstructure was also used, except for the final  
120 precipitation treatment of the  $\gamma'$  and  $\gamma''$  phases. To increase the size of the precipitates, an overaging  
121 process was applied at 750°C for 50 hours. Please note that throughout the rest of this article, a color  
122 code has been used to refer to the three microstructures: the *DA* microstructure is referenced in blue,  
123 the *CG* microstructure in red and *CGCP* microstructure in orange.

Ni	Fe	Cr	Mo	Al	Ti	Nb	Si	C
54.18	17.31	17.97	2.97	0.56	1	5.39	0.1	0.023

124 **Table 1. Composition of the Inconel 718 DA Alloy (Wt%).**

### 125 **1.2 Shot peening conditions**

126 The shot peened samples are parallelepipeds of 20x15x10 mm in size. The samples underwent  
127 mechanical polishing to achieve a mirror finish before shot peening. The aim was to reduce residual  
128 stresses and work hardening caused by machining. XRD measurements were conducted to confirm the  
129 absence of residual stress (see Section 2.2). The samples underwent shot peening on one of their

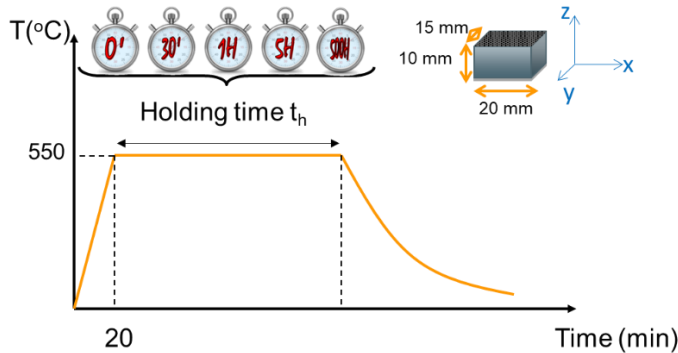
130 largest surfaces using a conventional nozzle and S110 steel shot. Two shot peening conditions (*SP1* and  
 131 *SP2*) were defined according to AFNOR standard NFL 06-832 [26]. The shot peening parameters (see  
 132 Table 2) were chosen for two reasons: (i) they are commonly applied to industrial components and (ii)  
 133 they induce very different residual stress and work hardening gradients, which is necessary to validate  
 134 the proposed methodology. The shot peening conditions were adjusted to take account for the fact  
 135 that the change in grain size results in a reduction in the strength of the modified microstructures. As  
 136 a consequence, the conditions shown in Table 2 were chosen so that the coverage was identical for all  
 137 three microstructures.

Name	Shot	Almen Intensity	Coverage
SP1	S110 steel	12-13A	125%
SP2	S110 steel	22-23A	200%

138 **Table 2. Shot peening conditions applied to the different microstructures.**

139 **1.3 Thermal loading conditions**

140 After shot peening, the samples were placed in a vacuum furnace and subjected to a temperature cycle  
 141 without any mechanical loading; Figure 1 illustrates the corresponding cycle. The rise in temperature  
 142 lasts 20 minutes; the temperature is then maintained at 550°C during a time lapse  $t_h$  called the “holding  
 143 time” in the present article. Five different holding times were applied in this experimental campaign,  
 144 ranging from 0 to 500 hours. The samples were then placed in an argon stream for rapid cooling. Note  
 145 that  $t_h = 0$  corresponds to a sample that has undergone an increase and a decrease in temperature  
 146 without any holding time.



147 **Figure 1. Diagram of the thermal loading cycle applied to the samples with the definition of the holding time.**

149  
 150

## 151 **1.4 Material characterization**

### 152 **1.4.1 Scanning Electron Microscope observations**

153 The microstructural observations were conducted using a MERLIN Scanning Electron Microscope (SEM)  
154 with an accelerating voltage of 5 kV and a nominal current of 40 nA. To reveal the microstructure,  
155 including the strengthening precipitates  $\gamma'$  and  $\gamma''$ , an ion polishing system was used to obtain a mirror-  
156 polished surface. The grain size was quantified using the Electron Backscattered Diffraction (EBSD)  
157 method. The data was acquired using a NORDIF CD camera operating at 30 fps coupled to a MERLIN  
158 SEM operating at 20 kV acceleration voltage and 40 nA nominal current.

### 159 **1.4.2 X-ray diffraction measurements**

160 X-ray diffraction measurements were conducted on the 311-diffraction peak at a  $2\theta$  angle of  
161 approximately  $111^\circ$  using a Seifert PTS diffractometer. The radiation source was a Co-K $\alpha$  tube with a  
162 wavelength of 1.79 Å, an accelerating voltage of 20 kV, and a nominal current of 4 mA. The sample  
163 preparation was identical to that used for microstructure characterization, as described above. Under  
164 these conditions, the X-ray penetration depth was estimated to be between 2 and 4  $\mu\text{m}$ , and the  
165 analyzed surface was a few millimeters wide. The X-ray data were processed using classical methods  
166 [27], specifically the  $\sin^2\psi$  method with analysis of eleven  $\psi$  angles to determine the depth profiles.  
167 Line broadening was used as a measure for work hardening (see Section 1.4.3 for more details). This  
168 was defined by the full width at half maximum (FWHM) of the peaks obtained by a Voigt pseudo-profile  
169 fit. For in-depth evaluation of the quantities of interest, electrolytic polishing with an average step of  
170 40  $\mu\text{m}$  was carried out. A correction method was applied which showed that the material removal had  
171 a negligible effect on the residual stress values. Residual stresses and peak widths were measured in  
172 two directions, but no significant differences were found. This confirms that shot peening induces an  
173 in-plane equi-biaxial stress state. The FWHM depth profile was evaluated before shot peening, and a  
174 consistent FWHM value was observed for all untreated samples, as shown by the triangular data points  
175 in Figure 5. After shot peening, three residual stress and FWHM profiles were determined at different  
176 locations on the surface of the samples for each microstructure to study the dispersion of these  
177 parameters. Following heat treatment, one residual stress and FWHM profile was measured for each  
178 microstructure.

### 179 **1.4.3 Procedure of work hardening characterization**

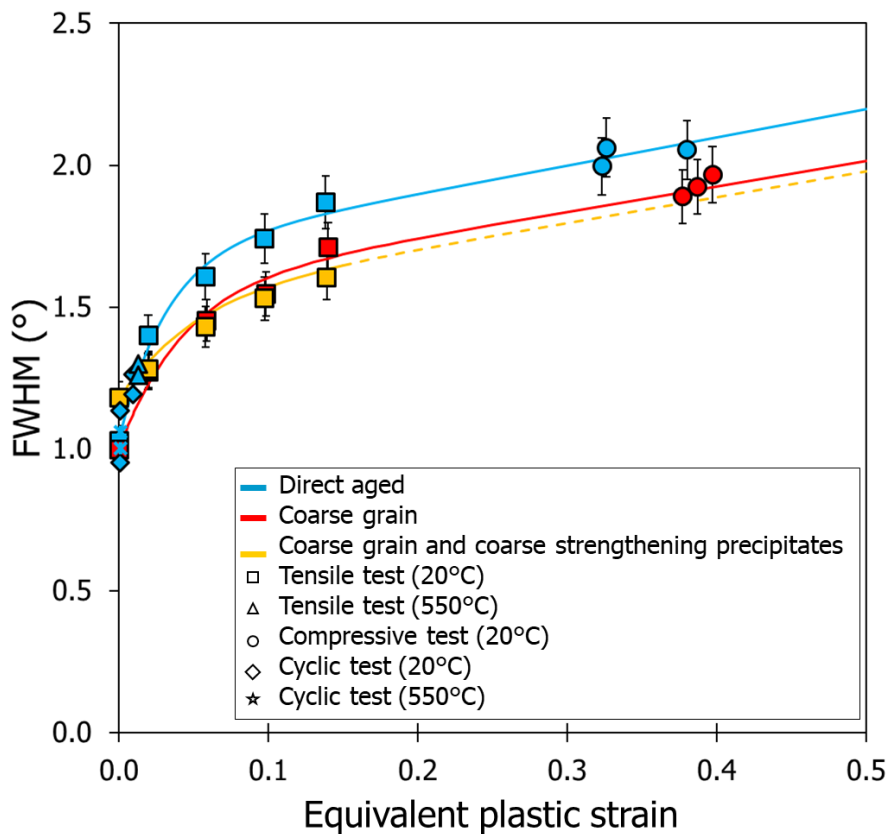
180 If the method for evaluating the residual stress values from X-Ray diffraction measurements is well  
181 established, the evaluation of the work hardening requires the implementation of a calibration method  
182 [17], [22], [28], [29], [30]. This method has been successfully applied to the microstructures studied in

183 this paper [11], [12] and has demonstrated its interest in validating the modeling of the shot peening  
 184 process [31]. Work hardening is identified with the equivalent plastic strain noted  $\varepsilon_p$  as discussed in  
 185 [11]. The relationship between the FWHM obtained by X-ray diffraction and the work hardening is  
 186 presented in Figure 2 for the three Inconel 718 microstructures and is modeled by [17]:

$$FWHM(\varepsilon_p) = A_{FWHM}(1 - e^{-B_{FWHM}\varepsilon_p}) + C_{FWHM} \varepsilon_p + D_{FWHM} \quad \text{Eq. 1}$$

187 The parameters that have been evaluated are  $A_{FWHM}$ ,  $B_{FWHM}$ ,  $C_{FWHM}$  and  $D_{FWHM}$  [11]. They are given in  
 188 Table 3. The work hardening induced by shot peening can be determined by inverting Eq. 1. A typical  
 189 work hardening profile obtained by this method is shown in Figure 3.

190 The parameters for the work hardening characterization were identified for each microstructure; this  
 191 method can be used only if no microstructural modification is observed during any of the treatments  
 192 (thermal or mechanical) that the samples undergo [11], [12]. Scanning electron microscope analyses  
 193 were therefore performed after shot peening and after the thermal treatment to assess the evolution  
 194 of the microstructure.



195  
 196 **Figure 2. The full width at half maximum (FWHM) as a function of equivalent plastic strain for different load**  
 197 **histories, temperatures, and microstructures with corresponding calibration curves. [11].**

198

	Direct Aged (DA)	Coarse grain (CG)	Coarse grain and coarse precipitates (CGCP)
$A_{FWHM}$	0.66	0.56	0.35
$B_{FWHM}$	31.12	23.92	20.00
$C_{FWHM}$	0.99	0.90	
$D_{FWHM}$	1.04	1.00	1.18

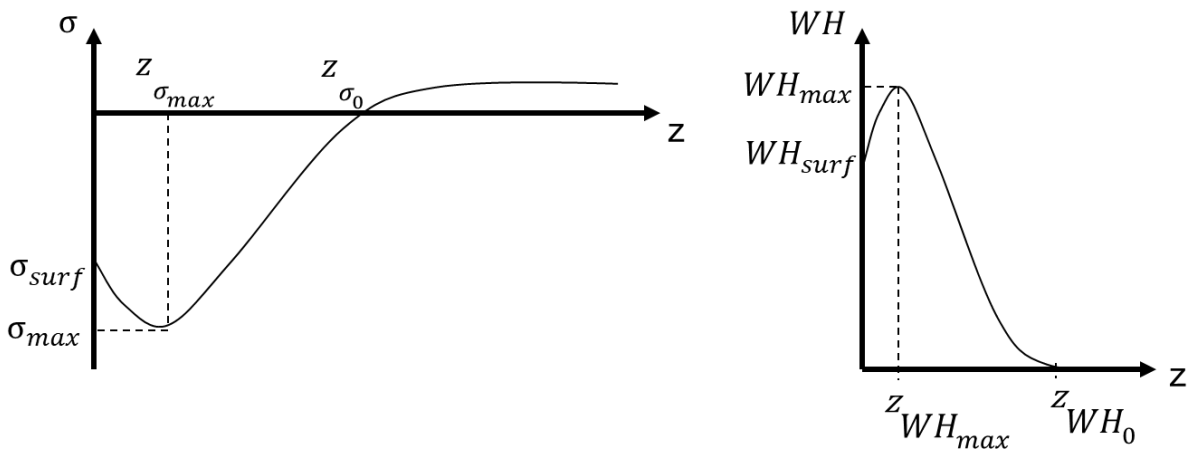
199 **Table 3.** The constants' values obtained for calibrating the full width at half maximum (FWHM) for the three  
 200 microstructures, as defined by Eq.1. [11]. Note that all constants are estimated to the nearest 0.01.

201 **1.4.4 Experimental plan**

202 To conclude this Materials and Methods Section, the complete X-ray diffraction measurement plan is  
 203 presented in Table 4. For each condition and each microstructure, the number of profiles acquired in  
 204 depth is indicated. Figure 3 also presents the syntax used to describe the shape of the shot peened  
 205 induced residual stress and work hardening profiles.

Holding time $t_h$ (h)	Microstructure								
	Direct Aged (DA)			Coarse grain (CG)			Coarse grain and coarse precipitates (CGCP)		
	Unshot	SP1	SP2	Unshot	SP1	SP2	Unshot	SP1	SP2
Untreated	3 p	3 p	3 p	3 p	3 p	3 p	3 p	3 p	3 p
0	-	1 p	1 p	-	1 p	1 p	-	1 p	1 p
0.5	-	1 p	1 p	-	1 p	1 p	-	1 p	1 p
1	-	1 p	1 p	-	1 p	1 p	-	1 p	1 p
5	-	1 p	1 p	-	1 p	1 p	-	1 p	1 p
50	-	1 p	1 p	-	1 p	1 p	-	1 p	1 p
500	-	1 pp	1 p	-	1 pp	1 pp	-	1 pp	1 pp

206 **Table 4.** X-ray diffraction measurement matrix. p: profile with measurements up to at least 300  $\mu\text{m}$  depth for  
 207 residual stresses and work hardening; pp: partial profile, up to 150  $\mu\text{m}$ .



208 **Figure 3.** Syntax used to describe the profiles of residual stress and work hardening induced by shot peening  
 209 induced.  
 210

## 211 **2 Experimental results**

### 212 **2.1 Microstructural observations**

213 To detect any microstructural evolution, SEM observations were carried out on the three investigated  
214 microstructures before shot peening, after shot peening alone, and after shot peening followed by a  
215 holding time of 500 hours at 550°C. The results of these observations are presented in Table 5. Only  
216 the results with the higher shot peening condition (*SP2*) are detailed here, as similar results were  
217 obtained for the *SP1* shot peening condition. Table 6 summarizes the microstructural characterizations  
218 obtained from SEM observations and EBSD analyses before shot peening. An average grain size of about  
219 5  $\mu\text{m}$  is observed for the *DA* microstructure, while the other two microstructures have average grain  
220 sizes around 35  $\mu\text{m}$ . The size of the strengthening precipitates is similar for the *DA* and *CG*  
221 microstructures (10 to 20 nm), but much larger for the *CGCS* microstructure with a size of 100 to 200  
222 nm. Binarization of the SEM images was performed to assess the morphology and distribution of the  $\delta$   
223 phase. A form factor of 0.9 was arbitrarily chosen to differentiate needle-shaped from globular  
224 precipitates. The proportion of the  $\delta$  phase in the *CG* and *CGCP* microstructures is between 1.4% and  
225 1.7%, values that remain in the same order of magnitude as for the *DA* microstructure (2.3%). The  
226 proportion of needles and globules (40% and 60%, respectively) is also similar for the three  
227 microstructures. Comparing the *DA* microstructure with the *CG* microstructure thus gives access to the  
228 effect of grain size. Similarly, the comparison of the *CG* and the *CGCP* microstructures allows studying  
229 the influence of the size of the strengthening precipitates.

230 The SEM characterization of a sample shot peened under *SP2* conditions, the most severe, shows a  
231 great stability of the microstructure (Figure 4). It confirms that the shot peening conditions applied in  
232 this work do not induce any change in grain size or orientation, or in the size of the strengthening  
233 precipitates. Similarly, the SEM characterization performed after the thermal loadings at 550°C  
234 revealed no microstructural change in terms of grain size or strengthening precipitate size, showing  
235 morphologically stable microstructures over time (Table 5). The temperature of 550°C used in this study  
236 for the thermal loading does not induce any microstructural change in the strengthening precipitates,  
237 even in the presence of work hardening at the material surface. It should be noted that an increase in  
238 the rate of  $\gamma''$  precipitates was observed in a previous study for shot peened samples subjected to aging  
239 treatments at 700°C [32]; this can be explained by the higher temperature of the treatment. These  
240 analyses validate that, since no microstructural change is observed, the calibration curves shown in  
241 Figure 2 can be used to evaluate the work hardening gradient introduced by shot peening, before and  
242 after the thermal loading.

		Before shot peening	After shot peening SP2 (Close to the surface)	After shot peening SP2 and 500h at 550°C (Close to the surface)
DA microstructure	Grains			
	Strengthening precipitates			
CG microstructure	Grains			
	Strengthening precipitates			
CGCP microstructure	Grains			
	Strengthening precipitates			

243

244

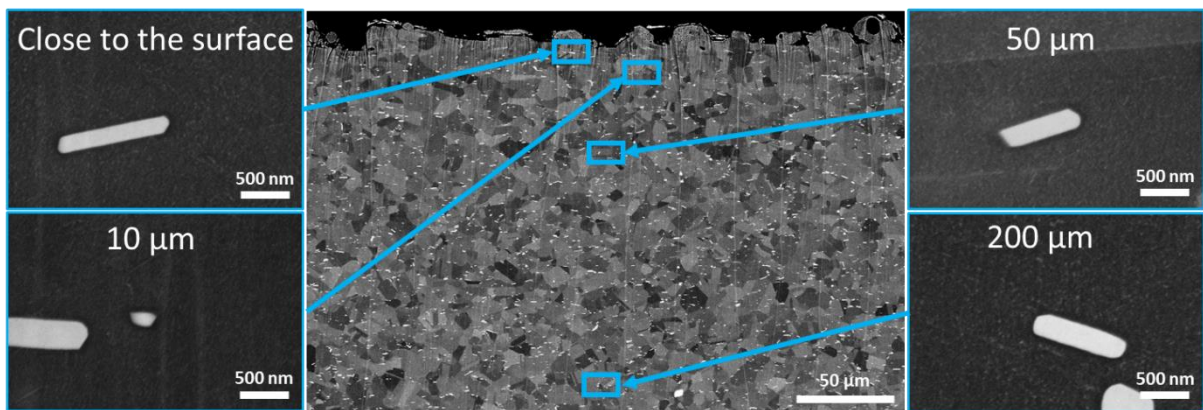
245

246

**Table 5. SEM microstructural characterizations carried out on the different microstructures: before shot peening, after shot peening (SP2) and after shot peening (SP2) and 500 hours at 550°C. The results obtained for the SP1 shot peening condition are similar.**

	Direct Aged microstructure	Coarse grain microstructure	Coarse strengthening precipitates microstructure
Average grain size ( $\mu\text{m}$ )	4.2	34.7	36.8
Strengthening precipitates size (nm)	$\sim 10 - 20$	$\sim 10 - 20$	$\sim 100 - 200$
$\delta$ phase area fraction	2.3%	1.4%	1.7%
$\delta$ phase morphology	$43 \pm 2\%$ needles $57 \pm 2\%$ globules	$36 \pm 2\%$ needles $64 \pm 2\%$ globules	$41 \pm 2\%$ needles $59 \pm 2\%$ globules

247 **Table 6. For the three investigated microstructures: mean size of the grain and of the strengthening**  
248 **precipitates, and  $\delta$  phase characteristics.**



249 **Figure 4. SEM images at different depth for DA microstructure after SP2 shot peening.**  
250

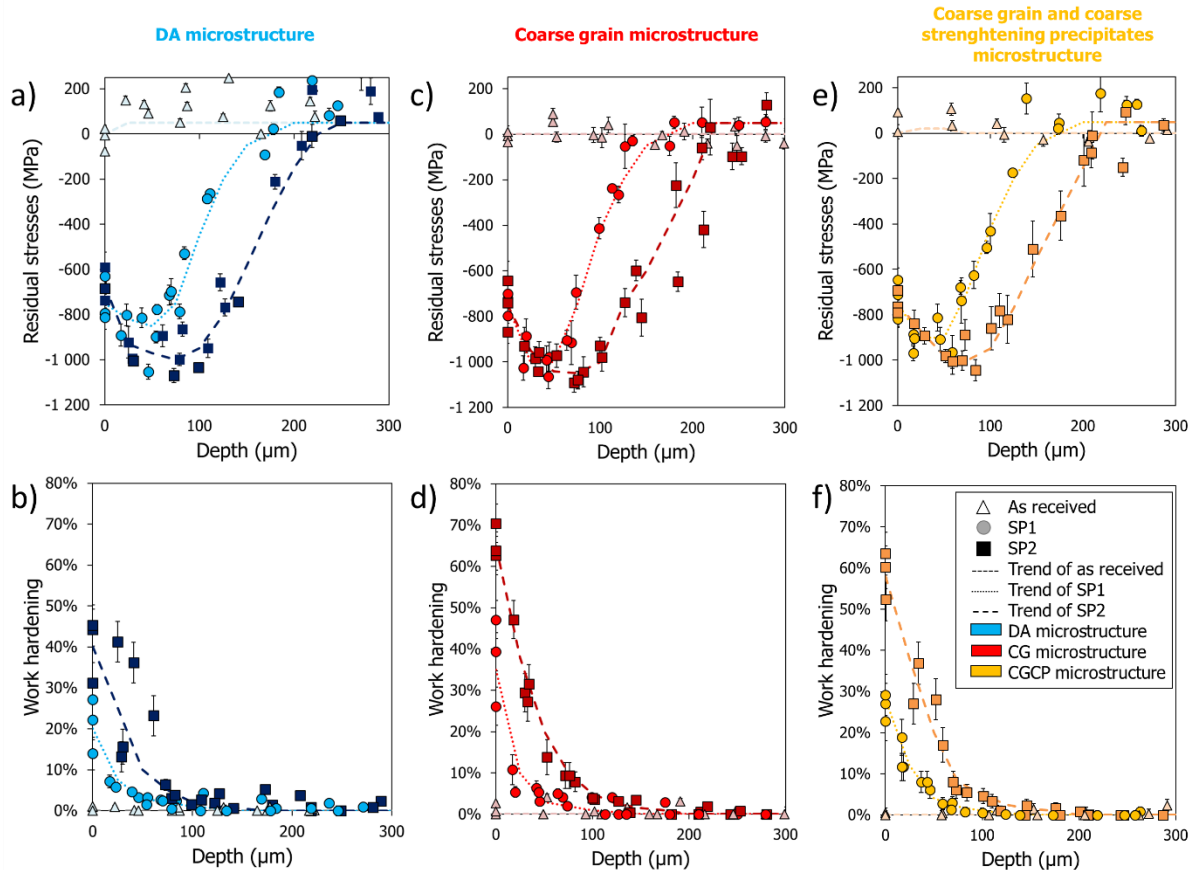
251

## 252 **2.2 Residual stresses and work hardening after shot peening**

253 The residual stress and work hardening profiles determined by X-ray diffraction for the three  
254 microstructures before shot peening and after SP1 and SP2 conditions are now compared (Figure 5).  
255 The dashed lines correspond to a fit obtained for each microstructure and each shot peening condition.  
256 Despite the fluctuations from one sample to another, clear trends are obtained between the two  
257 investigated shot peening conditions.

258 The work hardening is clearly affected by the shot peening conditions, both in terms of value and depth.  
259 For example, for the DA microstructure, the average surface value is changed by almost 50% between  
260 the SP1 and SP2 conditions ( $WH_{surf}^{\square} = 20\%$  and  $WH_{surf}^{\square} = 40\%$  respectively). An increase in shot  
261 peening coverage and intensity results in a higher maximum compressive residual stress  $\sigma_{max}^{\square}$ . The  
262 associated depth is also affected ( $z_{\sigma_{max}^{\square}SP1} = 50 \mu\text{m}$ ;  $z_{\sigma_{max}^{\square}SP2} = 80 \mu\text{m}$ ), as the size of the compression  
263 zone ( $z_{\sigma_0^{\square}SP1} = 175 \mu\text{m}$ ;  $z_{\sigma_0^{\square}SP2} = 225 \mu\text{m}$ ). At the surface, the residual stress values are relatively similar

264  $(\sigma_{surf}^{SP1} \approx \sigma_{surf}^{SP2} \approx -700 \text{ MPa})$ . Similar trends are observed for both *CG* and *CGCP* microstructures.  
 265 The residual stress differences remain below 100 MPa along the profiles when comparing the three  
 266 microstructures. Thus, changing the grain size or the strengthening precipitates size has little impact  
 267 on the residual stresses. However, the work hardening is strongly affected by the microstructural  
 268 modifications. An increase in grain size implies an increase in surface work hardening of more than 25%  
 269 for both investigated shot peening conditions. However, the thickness of the work hardened area is  
 270 only slightly altered.



271  
 272 **Figure 5. Residual stress and work hardening profiles determined by X-ray diffraction on the three**  
 273 **microstructures prior and after *SP1*, *SP2* peening conditions.**

274  
 275 These results highlight the influence of both the shot peening conditions and the microstructure on  
 276 the residual stress and work hardening profiles.

277 Table 7 presents the minimum and maximum values encountered for each condition for the *DA*  
 278 microstructure (see notations in Figure 3) with the purpose of characterizing experimental dispersion.  
 279 This experimental dispersion may come from: measurement errors, microstructural variation from one  
 280 sample to another, or the non-repeatability of the shot peening process. These three possible sources  
 281 of dispersion have been investigated and characterized. They are described in detail below.

- 282 - The measurement conditions are the same for all the samples, so the error is evaluated for all  
 283 measurements around 20 MPa. Therefore, the observed variations cannot be specifically due  
 284 to this aspect.
- 285 - Concerning the influence of the microstructure, the analyses in terms of grain size, distribution,  
 286 and size of strengthening precipitates or crystalline orientation do not show any notable  
 287 difference between the different samples. Looking at the *DA* microstructure compared to the  
 288 two modified microstructures, the small differences in terms of the average value of the  
 289 measured residual stresses or work hardening (Figure 5) show that the microstructural  
 290 variations, even of significant, can be neglected in front of the experimental variability related  
 291 to the shot peening itself.
- 292 - Indeed, it is classical observed that the shot peening process shows a wide scatter of  
 293 experimental residual stress results [23]. This dispersion is generally related to an inherent  
 294 variability of many parameters related to the shot stream, such as size, shape, hardness, impact  
 295 angle and shot peening time. One way to account for this dispersion is to use the Monte Carlo  
 296 simulation technique by introducing variability in the process parameters to predict the  
 297 residual stress field [33], [34]. The influence of the shot peening process on the repeatability  
 298 of the measurements appears to be the most detrimental aspect of the experimental  
 299 dispersion. Since it is difficult to control, a repetition of the measurements on different samples  
 300 is often recommended to obtain a better accuracy. Experimental standard deviations of the  
 301 order of 100 MPa for the residual stresses and of the order of 10% for the work hardening were  
 302 obtained at the surface for all the microstructures. The standard deviation seems to decrease  
 303 with depth. These results are consistent with those obtained by Daoud *et al.* in the simulation  
 304 of the shot peening process [35].

	SP1		SP2	
	Min	Max	Min	Max
$\sigma_{surf}^{\square}$ (MPa)	-600	-800	-600	-850
$\sigma_{max}^{\square}$ (MPa)	-800	-1050	-900	-1150
$z_{\sigma_{max}^{\square}}$ ( $\mu\text{m}$ )	40	60	70	90
$z_{\sigma_0^{\square}}$ ( $\mu\text{m}$ )	120	200	200	250
$WH_{max}^{\square}$ (%)	15	30	20	45
$WH_{surf}^{\square}$ (%)	15	30	20	45
$z_{WH_{max}^{\square}}$ ( $\mu\text{m}$ )	0	0	0	0
$z_{WH_0^{\square}}$ ( $\mu\text{m}$ )	75	170	100	200

305 **Table 7. Summary of variations encountered for the two SP1 and SP2 shot peening conditions for the DA**  
 306 **microstructure.**

## 307 **2.3 Residual stresses and work hardening after a thermal loading**

308 The residual stresses and work hardening determined after thermal loading are now being studied. The  
309 first part is devoted to the study of the profiles. The second part focuses on the evolution of the key  
310 parameters identified in Figure 3, which will serve as the basis for a model to estimate the relaxation  
311 of residual stresses.

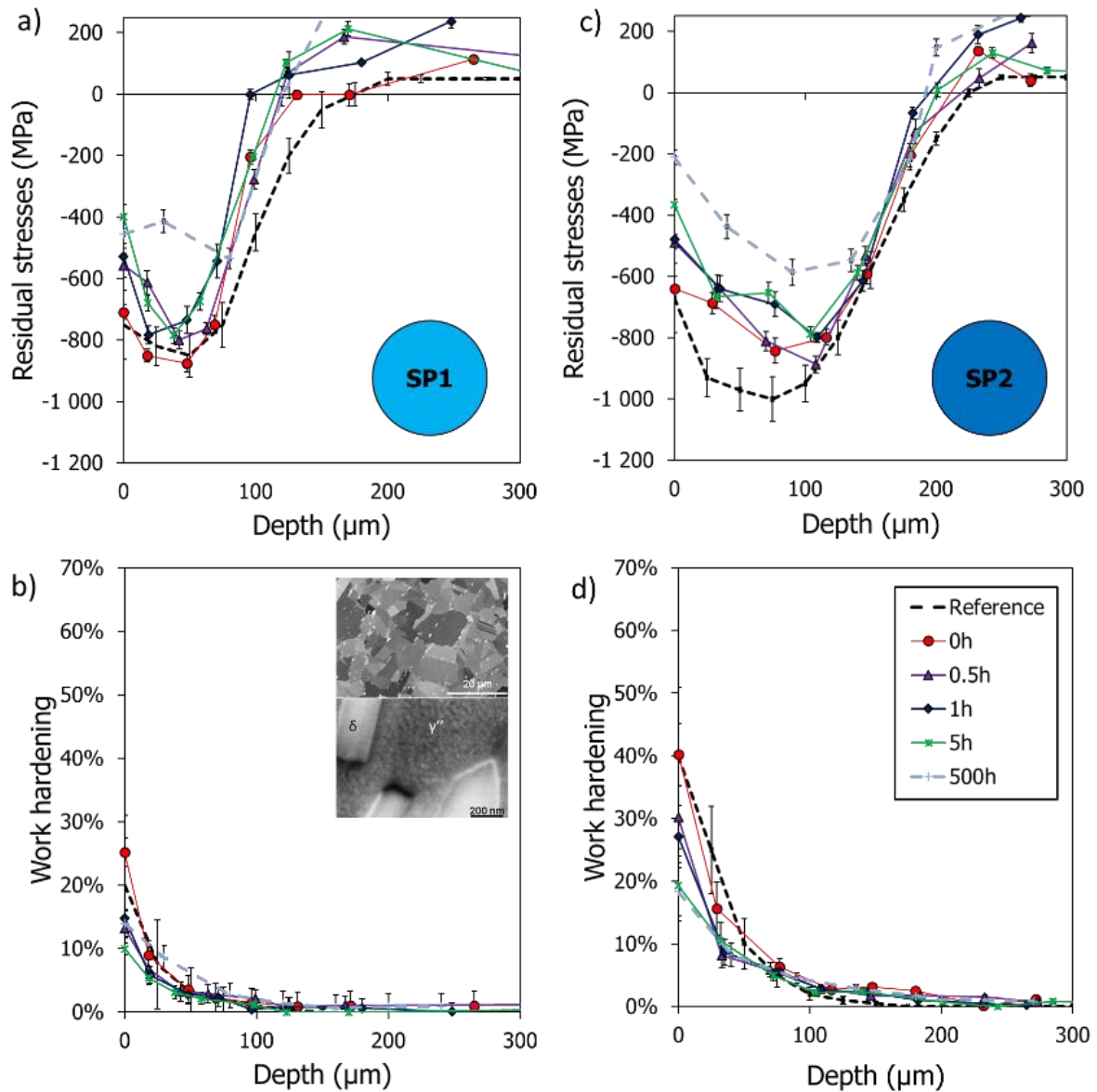
### 312 **2.3.1 Residual stress and work hardening profiles after thermal loading**

313 The residual stress and work hardening profiles were analyzed to track their evolution after the shot  
314 peened samples were subjected to different holding times at 550°C. As the relaxation under thermal  
315 loading is isotropic, only the component in the  $\vec{x}$  direction of the stress was studied (see caption of  
316 Figure 1). Note that a distinction is made between samples that have not undergone thermal loading  
317 and those that have undergone a temperature rise and fall ( $t_h = 0$ ). Except for a few measured points  
318 related to the *SP2* shot peening condition, the difference is small between the reference and the  
319 samples that have undergone a holding time  $t_h = 0$ : the rise and fall in temperature do not trigger any  
320 relaxation.

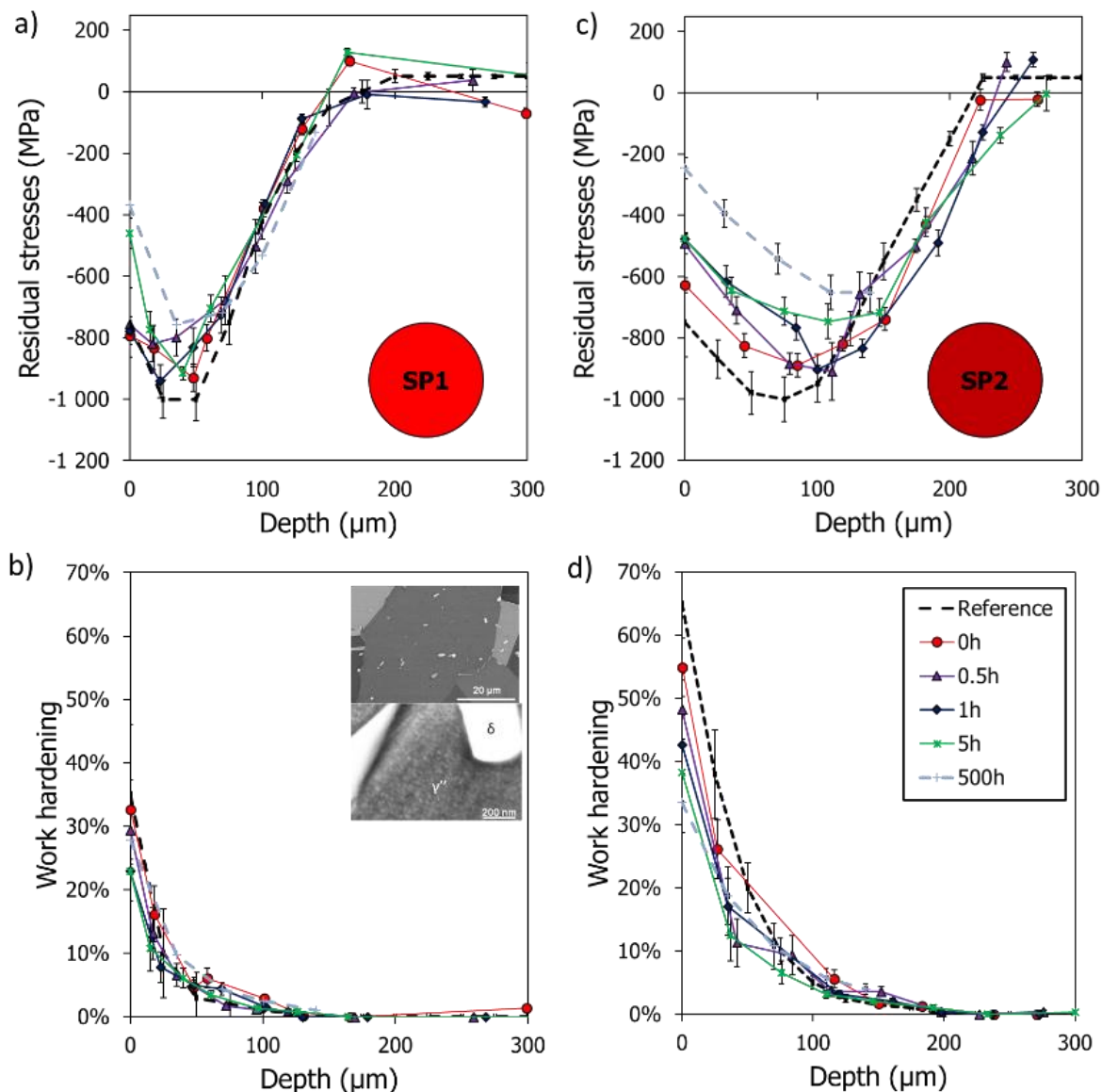
321 Figure 6 shows the residual stress and work hardening profiles obtained after thermal loading for the  
322 *DA* microstructure, shot peened under *SP1* (Figure 6.a and b.) and *SP2* (Figure 6.c and d.) conditions.  
323 Both shot peening conditions present the same evolution of the profiles. The residual stresses and  
324 work hardening induced by shot peening are only partially relaxed during thermal loading, even for the  
325 longest holding times. The depth associated with the maximum value of compressive residual stresses  
326  $z_{\sigma_{max}}$  is not affected by the duration of the thermal holding at 550°C. On the contrary, for the *SP1*  
327 condition, the depth at which the residual stresses become positive  $z_{\sigma_0}$  undergoes a slight decrease  
328 with a holding time at 550°C, which is not observed for the *SP2* conditions. It is interesting to note that  
329 the surface residual stress that corresponds to the most intense level of work hardening, experiences  
330 the greatest relaxation. This relaxation is even more pronounced for the *SP2* condition: at the surface  
331 where the work hardening value is about 40%, the compressive residual stress value evolves from -600  
332 MPa to -200 MPa.

333 Figure 7 and Figure 8 show the residual stress and work hardening profiles for the *CG* and *CGCP*  
334 microstructures, respectively. It is noteworthy for these modified microstructures that even at very  
335 high levels of surface work hardening (over 60% for the *CG* and *CGCP* microstructures under *SP2*  
336 conditions), the relaxation of residual stresses is only partial after several hundred hours at 550°C.  
337 Again, the depth associated with the maximum value of compressive residual stresses  $z_{\sigma_{max}}$  and that  
338 at which the residual stresses are positive  $z_{\sigma_0}$  appear to be relatively unaffected by the increase  
339 holding time. Similar to what was observed in the *DA* microstructure, the higher the level of work

340 hardening, the higher the relaxation of residual stresses. The highest levels of relaxation are then found  
 341 at the surface.  
 342 The main information to be drawn from these results is that the effects of shot peening, although  
 343 partially reduced, are still present even after being exposed to a purely thermal loading at 550°C for  
 344 several hundred hours. It is therefore of particular interest to be able to model the residual stress  
 345 relaxation at any point on the part, in order to know the residual stress profile at any point in time.



346  
 347 **Figure 6. Residual stress and work hardening profiles, for different holding times at 550°C, for Inconel 718 DA**  
 348 **microstructure, SP1 and SP2 conditions.**

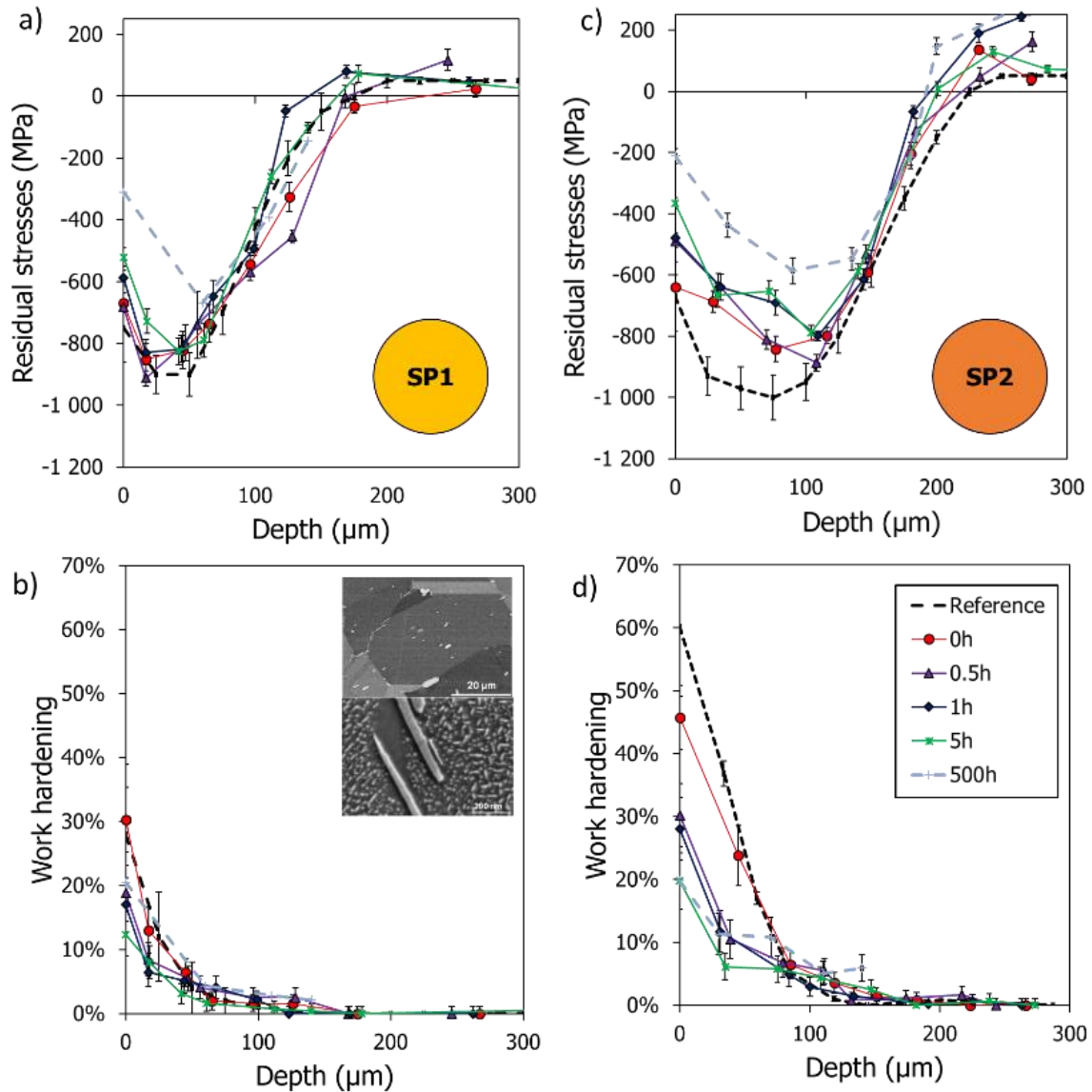


349

350

351

Figure 7. Residual stress and work hardening profiles for different holding times at 550°C, for Inconel 718 coarse grain microstructure, SP1 and SP2 conditions.



352

353

**Figure 8. Residual stress and work hardening profiles for different holding times at 550°C, for Inconel 718 coarse grain and coarse strengthening microstructure, SP1 and SP2 conditions.**

354

### 355 2.3.2 Definition of ratios to quantify relaxation

356 Ratios are here defined to quantify the relaxation of the residual stresses and the work hardening due  
 357 to thermal loading. We first define reference profiles corresponding to the profiles determined after  
 358 shot peening, for which, by definition, there is no relaxation. These reference profiles are respectively  
 359 noted,  $\sigma_{ref}(z)$  for the residual stresses and  $WH_{ref}(z)$  for work hardening. The experimental reference  
 360 profiles are all presented in Figure 5 as a function of the depth  $z$  for different microstructures and shot  
 361 peening conditions.

362 Several profiles of residual stress and work hardening were evaluated after thermal loading for different  
 363 holding times  $t_h$  (see Figure 1 for the definition of  $t_h$ ). These profiles are noted  $\sigma(t_h, z)$  for the residual  
 364 stresses and  $WH(t_h, z)$  for work hardening, respectively, and are presented in Figure 6 to Figure 8 as a

365 function of the depth  $z$  for different microstructures and shot peening conditions.

366 To quantify the relaxation, we define the ratios  $R^\sigma(t_h, z)$  for residual stresses and  $R^{WH}(t_h, z)$  for work  
367 hardening such that:

$$R^\sigma(t_h, z) = \frac{\sigma(t_h, z)}{\sigma_{ref}(z)} \quad \text{and} \quad R^{WH}(t_h, z) = \frac{WH(t_h, z)}{WH_{ref}(z)} \quad \text{Eq. 2}$$

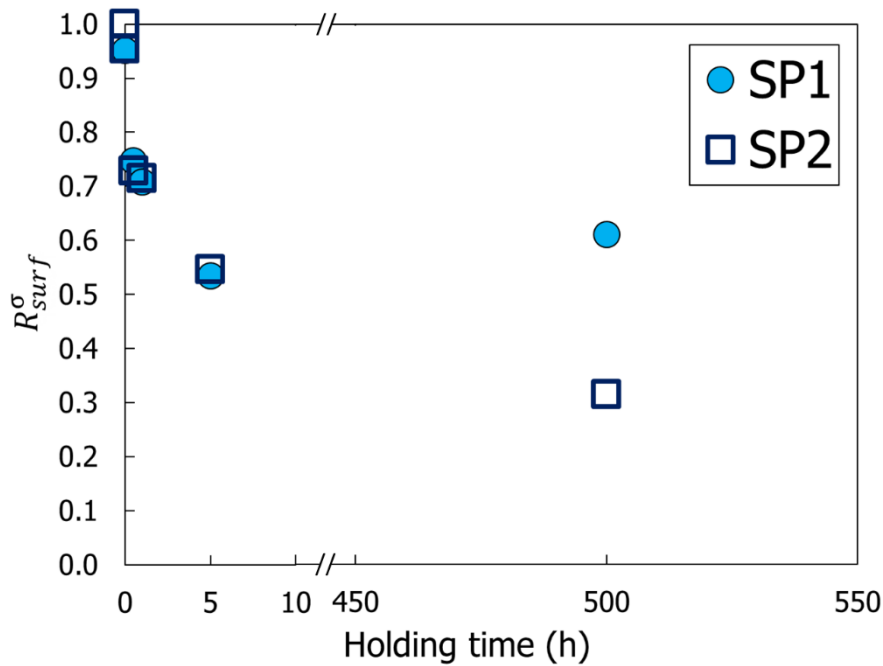
368 Thus, when the ratios are equal to 1, no relaxation is observed; if the ratios were equal to 0, all the  
369 residual stresses or work hardening would have vanished.

### 370 **2.3.3 Evolution of the surface and maximum values of residual stresses and** 371 **work hardening with thermal loading**

372 To simplify the analysis, representative points have been identified on the profiles of the residual stress  
373 and work hardening shown in Figure 6 to Figure 8. The evolution of these specific values is here studied  
374 as a function of the holding time  $t_h$ . For residual stress, the surface residual stress  $\sigma_{surf}^{\square}$  and the  
375 maximum value  $\sigma_{max}^{\square}$  at depth  $z_{\sigma_{max}^{\square}}$  were considered. For work hardening, the value at the surface  
376  $WH_{surf}^{\square}$  alone has been considered since work hardening is maximum at the surface (see Figure 3 for  
377 the definition of  $\sigma_{surf}^{\square}$ ,  $z_{\sigma_{max}^{\square}}$  and  $WH_{surf}^{\square}$ ). The following ratios as detailed in Section 2.3.2 can then  
378 be defined:

$$R_{surf}^\sigma(t_h) = \frac{\sigma(t_h, 0)}{\sigma_{ref}(0)} \quad R_{max}^\sigma(t_h) = \frac{\sigma(t_h, z_{\sigma_{max}^{\square}})}{\sigma_{ref}(z_{\sigma_{max}^{\square}})} \quad R_{max}^{WH}(t_h) = \frac{WH(t_h, 0)}{WH_{ref}(0)} \quad \text{Eq. 3}$$

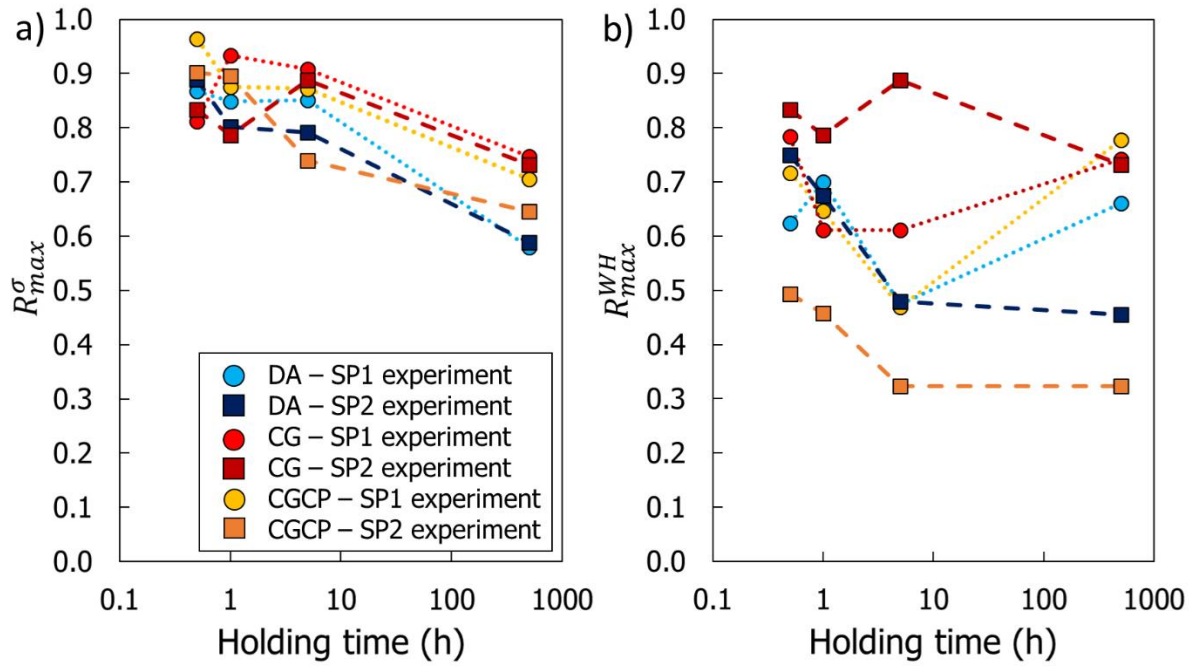
379 The evolution of  $R_{surf}^\sigma$  as a function of holding time is shown in Figure 9 for the *DA* microstructure and  
380 the two shot peening conditions. A significant evolution of the surface residual stresses occurs in the  
381 early stages (before 5 hours); between 5 and 500 hours, the surface residual stresses relax at a  
382 significantly lower rate. Very similar results were obtained for the other two microstructures and are  
383 thus not presented here.



384

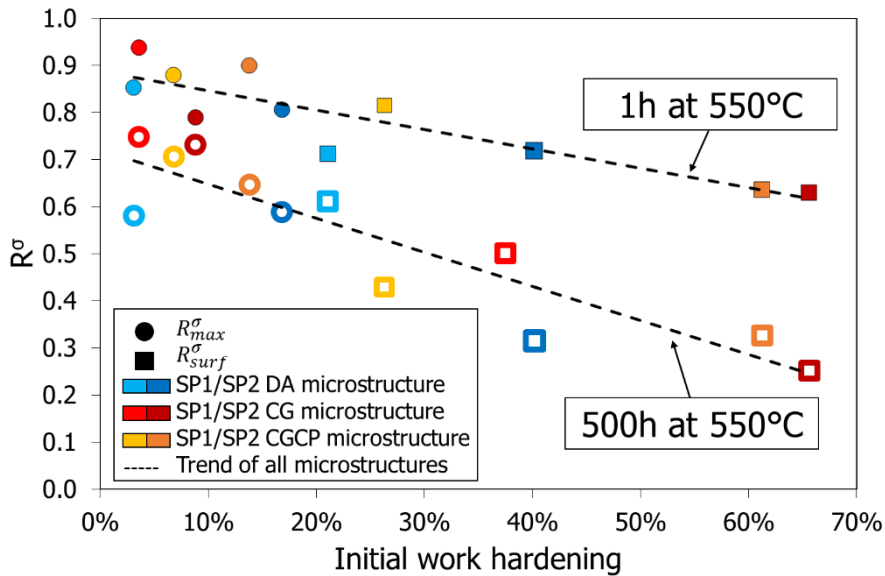
385 **Figure 9. Evolution of  $R_{surf}^{\sigma}$  as a function of time at 550°C for the DA microstructure and the two SP1 and SP2**  
 386 **shot peening conditions; note the change in scale for the smaller holding time axis.**

387 The evolutions of  $R_{max}^{\sigma}$  and  $R_{max}^{WH}$  are shown in Figure 10 as a function of holding time, for the three  
 388 microstructures and the two shot peening conditions; note that a logarithmic scale has been adopted  
 389 for the holding time. As a whole, the results enable to identify some trends concerning the evolution  
 390 of the different variables as a function of holding time (note the scale is logarithmic): (i) a significant  
 391 evolution of the maximum residual stresses and work hardening occurs for holding times below 5  
 392 hours; this was also observed for the surface residual stress; (ii) for holding times above 5 hours, the  
 393 relaxation of the residual stresses is reduced and the work hardening is slowed down, particularly for  
 394 SP2. Comparing Figure 9 and Figure 10, it is also clear that  $R_{max}^{\sigma}$  is higher than  $R_{surf}^{\sigma}$ . For example, for  
 395 the DA microstructure, SP2 shot peening condition, and after a holding time  $t_h = 5h$ ,  $R_{max}^{\sigma} = 0.8$  while  
 396  $R_{surf}^{\sigma} = 0.55$ . This means that the relaxation of residual stresses is maximum at the surface. These  
 397 results are related to the initial work hardening value introduced during shot peening. The higher the  
 398 work hardening value, the higher the relaxation of the residual stresses. To visualize this, the values  
 399  $R_{surf}^{\sigma}$  and  $R_{max}^{\sigma}$  can be plotted as a function of the initial work hardening. Figure 11 presents the results  
 400 obtained for two holding times (1 h and 500 h). For a given holding time, a linear relationship is  
 401 obtained between the normalized unrelaxed residual stress  $R^{\sigma}$  and the initial work hardening. The  
 402 longer the holding time, the greater the influence of work hardening. It is interesting to note that the  
 403 three microstructures follow a very similar trend. These results show work hardening is the dominant  
 404 parameter in the relaxation of residual stresses. The influence of the microstructure on the relaxation  
 405 of the residual stresses is only of second order.



406  
407  
408

Figure 10. Evolution of a)  $R_{max}^{\sigma}$  and b)  $R_{max}^{WH}$  as a function of holding time at 550°C for the three microstructures and the two shot peening conditions.



409  
410  
411  
412

Figure 11. Evolution of  $R^{\sigma}$  as a function of the initial work hardening value.  $R_{surf}^{\sigma}$  and  $R_{max}^{\sigma}$  values are indicated by circles and squares respectively. The definition of these parameters is given in Eq. 3. Only results for two holding times (1h and 500h) are presented.

### 413 2.3.4 Influence of the microstructure

414 If we want to identify the second order influence of the microstructure on the relaxation of residual  
415 stresses, it is necessary to remove the influence of work hardening. To do this, it is essential to analyze  
416 points with similar work hardening levels, or at least with sufficiently low work hardening levels, so

417 that this parameter has the minimum impact on the analysis. It is interesting to notice that, for the  
418 depth  $z_{\sigma_{max}}$ , work hardening is five times lower than the surface work hardening (see for example  
419 Figure 6). Moreover, it is relatively similar for the two shot peening conditions and the three  
420 microstructures (comparing Figure 6 to Figure 8). The influence of the microstructure can then be  
421 determined by observing the evolution of  $R_{max}^{\sigma}$  (Figure 10.a). A holding time of 500 h is chosen to  
422 analyze the results because the effects are more pronounced in this case. The results are shown in  
423 Table 8. An increase in grain size leads to a decrease in the thermal relaxation of residual stresses. The  
424 influence of a change in the size of the strengthening precipitates is more questionable. An increase in  
425 the size of the precipitates leads to a slight increase in the relaxation of residual stresses.

426 To explain this dependence on the microstructure, we consider the mobility of dislocations.  
427 Dislocations are the main vector of the plastic deformation introduced into the microstructure by shot  
428 peening. Because of the strong plastic strain introduced during the process, a rearrangement of the  
429 dislocations towards lower distortion energies occurs during the first moments at high temperature  
430 [23]. The more the dislocation structure is disturbed, the more it has to rearrange itself to reach an  
431 equilibrium level. This reorganization within the material leads to a relaxation of the residual stresses.  
432 The phenomena observed here are of the recovery process type. However, similarities can be drawn  
433 from studies dealing with the influence of microstructure on the creep behavior of Inconel 718. For a  
434 creep load, it has been shown in the literature that the influence of microstructural parameters in order  
435 of importance in Inconel 718 are: grain size, morphology and distribution of the  $\delta$  phase and the size  
436 of the strengthening precipitates  $\gamma'/\gamma''$  [7], [8], [9]. As the grain size increases, the linear density of grain  
437 boundaries decreases, leading to a limitation of grain boundary slip and diffusion mechanisms at high  
438 temperatures. The  $\delta$  phase appears to be the most important microstructural parameter on creep at  
439 an equivalent grain size. The lower the proportion of  $\delta$  phase at the grain boundaries, the better the  
440 creep resistance. Moreover, a globular morphology is to be preferred to an acicular one to limit creep  
441 [7]. Finally, the size of the strengthening precipitates  $\gamma'/\gamma''$  can play a major role at fixed grain size and  
442  $\delta$  phase fraction, depending on the structural hardening mechanism involved. In the modified  
443 microstructures of this study, the transition from *DA* to *CG* microstructure mainly leads to an increase  
444 in grain size by a factor of 5 (see Table 5). Thus, the differences observed between the *DA* and *CG*  
445 microstructures are essentially related to the increase in grain size. Grain size,  $\delta$  phase density, and  
446 distribution are similar between the two modified microstructures (*CG* and *CGCP*). The size of the  
447 strengthening precipitates is the only factor that causes a factor of ten difference between the two  
448 microstructures. According to Sundararaman, the size of the strengthening precipitates that causes a  
449 change in the precipitate shearing mechanisms is around 10 nm in the case of Inconel 718 [36]. In the  
450 present work, the size of the precipitates is greater than this value (20 and 200 nm see Table 6) for all

451 the studied microstructures, so that a bypass type of Orowan mechanism occurs. When a dislocation  
 452 bypasses an obstacle, it may create more dislocations. These newly formed dislocations are usually  
 453 mobile and can move through the crystal lattice. This mechanism can thus increase the number of  
 454 mobile dislocations in the material [36]. As a result, during holdings at 550°C, the dislocations rearrange  
 455 more easily as the size of the precipitates increases. This leads to an easier return to an equilibrium  
 456 state and, thus, to a more significant relaxation of the residual stresses. However, since the impact of  
 457 the size of the strengthening precipitates is of third order, the influence of a modification of their size  
 458 on the relaxation of the residual stresses appears to be moderate in this work, and this despite a factor  
 459 of 10 between the two modified microstructures.

	Direct Aged microstructure	Coarse grain microstructure	Coarse strengthening precipitates microstructure
SP1	0.59	0.75	0.71
SP2	0.59	0.73	0.65

460 **Table 8. Value of  $R_{max}^{\sigma}$  after 500 hours of holding time at 550°C for the three microstructures and the two**  
 461 **shot peening conditions.**

462

### 463 **3 A model for the thermal relaxation of residual stresses**

464 The experimental results section confirms the previously obtained results in the literature [14], [15],  
 465 [16], [37]. It also clearly demonstrates the influence of work hardening on residual stress relaxation. It  
 466 is now proposed to build on these results to provide a model that allows the assessment of residual  
 467 stress relaxation. The first proposal is to evaluate the existing Zener-Wert-Avrami model using these  
 468 data. Then, a new model considering work hardening is proposed. The model's validation is conducted  
 469 by comparing it with our experimental data and complementary results from the literature. Finally, an  
 470 example is provided to demonstrate the model's application.

#### 471 **3.1 The Zener-Wert-Avrami model**

472 The Zener-Wert-Avrami model is an empirical equation widely used in the literature to describe the  
 473 evolution of a thermally activated process [38]. It was first used by Vöhringer in 1987 to describe the  
 474 relaxation of residual stresses [23]. Since its introduction, this model has been used by many authors  
 475 on different materials (steels, nickel-based alloys, titanium and aluminum alloys) [16], [20], [23], [24],  
 476 [25]. This model allows for the determination of the stress relaxation  $\sigma(T, t_h)$  at a given depth relative  
 477 to the initial stress at the same depth  $\sigma_{ref}^{\square}$ , as a function of the holding time  $t_h$  and the temperature  $T$   
 478 using the following equation:

$$\frac{\sigma(T, t_h)}{\sigma_{ref}} = \exp\left(-\left[C \exp\left(-\frac{\Delta H_A}{k T}\right) t_h\right]^m\right) \quad \text{Eq. 4}$$

479 where  $\Delta H_A$  is the activation enthalpy,  $k$  is the Boltzmann constant,  $C$  and  $m$  are material parameters to  
 480 be identified for each position in the component.

481 In this work, since the tests are all performed at the same temperature, Eq. 4 is reduced to:

$$\frac{\sigma(t_h)}{\sigma_{ref}} = \exp(-[A \cdot t_h]^m) \quad \text{Eq. 5}$$

482  $A$  and  $m$  have then to be identified for each manufacturing process, each microstructure, and each  
 483 point in the structure.

484 To evaluate the ability of the Zener-Wert-Avrami model to reproduce the experimental results of the  
 485 present study, the parameters  $A$  and  $m$  have been identified for the experimental data presented  
 486 Section 2; a least square method has been applied for each microstructure, for each shot peening  
 487 condition and for each position,  $Z_{\sigma_{surf}}^{RS}$  and  $Z_{\sigma_{max}}^{RS}$ . The corresponding sets of values for  $A$  and  $m$  are  
 488 presented in Table 9. Note that the parameters obtained,  $A$  and  $m$ , are simply the values that best fit  
 489 the proposed empirical (Eq. 5) for predicting residual stress relaxation. No physical meaning can be  
 490 attached to these values. As expected, these values depend on the shot peening conditions and the  
 491 microstructure. Note that the  $m$  parameter is the most affected by the position and thus by work  
 492 hardening. The Zener-Wert-Avrami model is mainly devoted to the prediction of relaxation as a function  
 493 of the temperature. Due to the substantial impact of work hardening on the thermal relaxation of  
 494 residual stresses, and the large range of hardening in the structure induced by shot peening, this model  
 495 is not suitable for the description of the thermal relaxation of a complete residual stress profile or  
 496 others shot peening conditions.

Parameter	Depth	DA-SP1	DA-SP2	CG-SP1	CG-SP2	CGCP-SP1	CGCP-SP2
A	$Z_{\sigma_{surf}}^{\square}$	6.56E-02	1.91E-01	8.21E-02	2.05E-01	3.17E-01	1.43E-01
	$Z_{\sigma_{max}}^{\square}$	1.96E-01	1.88E-01	1.24E-01	6.82E-02	2.57E-01	2.11E-01
m	$Z_{\sigma_{surf}}^{\square}$	3.04E-07	5.59E-03	2.31E-05	6.84E-03	1.96E-03	3.03E-03
	$Z_{\sigma_{max}}^{\square}$	6.28E-05	8.11E-05	2.52E-08	9.89E-12	4.95E-05	7.40E-05

497 **Table 9. Values of the coefficients identified for the different shot peening conditions and the different**  
 498 **microstructures at two depths ( $Z_{\sigma_{surf}}^{\square}$ ,  $Z_{\sigma_{max}}^{\square}$ ).**

### 499 **3.2 A model for thermal residual stress relaxation accounting for work** 500 **hardening**

501 A model, which considers the work hardening state and considers holding time and position, is  
 502 proposed to predict the relaxation of residual stresses. This model is based on the experimental  
 503 observations presented in Section 2. The aim of the model is to be independent of the manufacturing

504 process that generated the residual stresses. In addition, its relative simplicity (analytical) is crucial to  
 505 function as a practical tool for validating the conditions of a prestressing manufacturing process and its  
 506 parameters in an industrial context. It has been shown that the microstructural impact on the thermal  
 507 relaxation of residual stresses is small compared to that of work hardening (see Section 2.3). It is thus  
 508 decided to disregard the influence of the microstructure to define the model. We then study the  
 509 residual stress ratio  $R^\sigma$  (defined Eq.3) at two specific locations  $z_{\sigma_{surf}}$  and  $z_{\sigma_{max}}$  as a function of the  
 510 initial work hardening level. These results are presented in Figure 12 for all the investigated holding  
 511 times; note that in this figure, the microstructure has not been identified to simplify the reading since  
 512 we disregard its influence. Shot peening conditions are considered on the basis of the level of work  
 513 hardening they cause. Therefore, in the same way, they are not explicitly shown in Figure 12. A linear  
 514 regression has been conducted for the data points corresponding to each specified holding time.  
 515 Comparing the experimental results and the straight line obtained with the linear regression, we make  
 516 the hypothesis that, for a given holding time, the ratio of unrelaxed residual stresses depends linearly  
 517 on the initial value of the work hardening and can be expressed as follows:

$$R^\sigma(t_h, z) = B(t_h) \cdot WH(z) + C(t_h) \quad \text{Eq. 6}$$

518 where  $WH(z)$  is the initial work hardening value at the depth  $z$  (with a range between 0 and 1) and,  
 519  $B(t_h)$  and  $C(t_h)$  are functions that depend on the holding time.

520 The parameters  $B$  and  $C$  are evaluated for each straight line in Figure 12 and for each holding time; the  
 521 corresponding results are shown in Figure 13. These two parameters exhibit a rapid evolution for the  
 522 shorter holding times, followed by a stabilization for the longest holding time. It is therefore proposed  
 523 to describe the evolution of  $C(t_h)$  and  $B(t_h)$  with a logarithmic function such that:

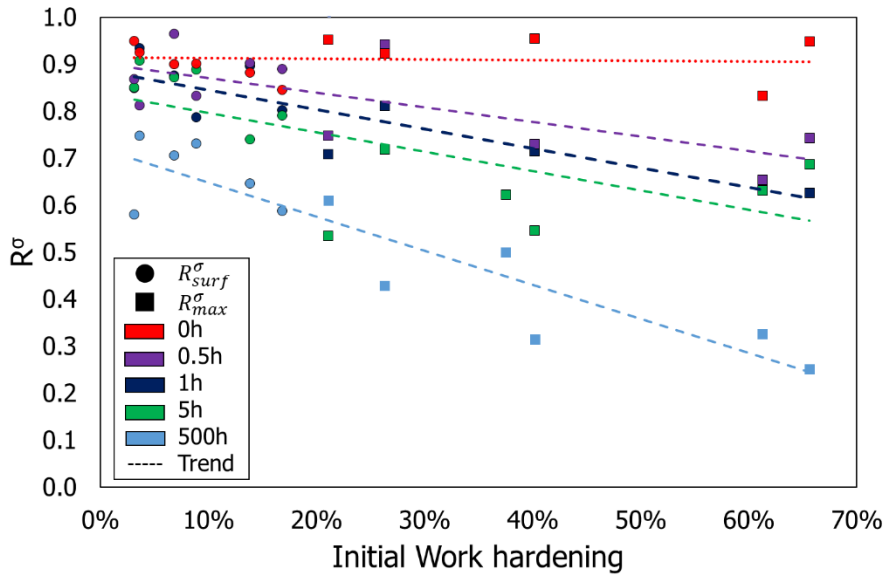
$$B(t_h) = b_1 \log_{10}(t_h) + b_2 \quad \text{Eq. 7}$$

$$C(t_h) = c_1 \log_{10}(t_h) + c_2 \quad \text{Eq. 8}$$

524 with  $b_1, b_2, c_1$  and  $c_2$  being constant parameters that need to be identified. Considering this formulation,  
 525 for  $t_h = 0$ , the model gives  $B(0) \neq 0$  and  $C(0) \neq 1$ . Therefore, the model may appear erroneous for holding  
 526 times less than 0.029 hours (i.e., 2 minutes). However, given the holding times used in the proposed  
 527 applications (greater than 30 minutes), and in the interest of model simplicity, this model is considered  
 528 in the following, as is Eq. 6. Other formulation using exponential function could be used to respect that  
 529 the residual stress profile being then the initial one as expected ( $B(0) = 0$  and  $C(0) = 1$ ).

530 Also note that in the model a residual stress relaxation can be obtained even if there is no work hard-  
 531 ening ( $WH(0) = 0$ ) in the material. Finally, the proposed model that estimates the ratio of unrelaxed  
 532 residual stresses takes the form:

$$R^\sigma(t_h, z) = [b_1 \log_{10}(t_h) + b_2] \cdot WH(z) + c_1 \log_{10}(t_h) + c_2 \quad \text{Eq. 9}$$

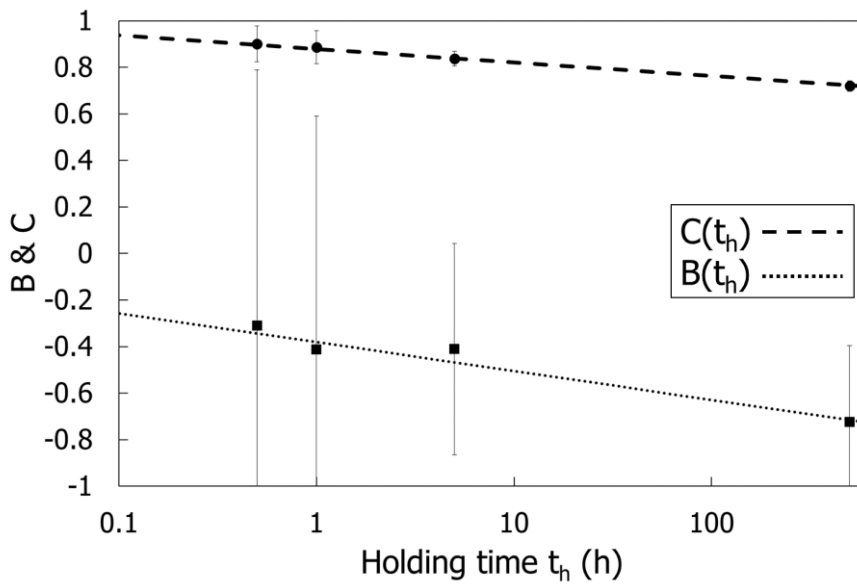


533

534

535

Figure 12. Evolution of  $R^\sigma$  as a function of the initial work hardening level without distinction of microstructure and for different holding times and for the two depth locations  $z_{\sigma_{surf}}$  and  $z_{\sigma_{max}}$ .



536

537

Figure 13. Evolution of  $B(t_h)$  and  $C(t_h)$  as a function of holding time.

538

539

540

541

542

543

The four material parameters  $b_1$ ,  $b_2$ ,  $c_1$  and  $c_2$  have been identified for Inconel 718 with a least square method on the data presented in Figure 13. The obtained values are given in Table 10. Note that given the model form in Eq.9, only three holding time values are sufficient to identify the model, such as the initial residual stress and work hardening levels and the residual stress and work hardening levels after 5 hours and 500 hours of holding time.

$b_1$	$b_2$	$c_1$	$c_2$
-0.130	-0.364	-0.061	0.907

544 **Table 10. Values of the parameters of the model of Eq. 9 for Inconel 718.**

545 Note that the parameters  $B(t_h)$  and  $C(t_h)$  could be modified to include a dependence on temperature.  
 546 By considering different temperatures in an experimental campaign, an exponential form with temper-  
 547 ature dependence could be considered for these parameters. This constitutes a perspective on the  
 548 present work.

### 549 **3.3 Model validation**

550 The model proposed in the previous section is now employed to predict the relaxation of residual  
 551 stresses under varying conditions. These conditions differ from those of the previous analysis used to  
 552 identify the parameters. Three sets of experimental data are considered:

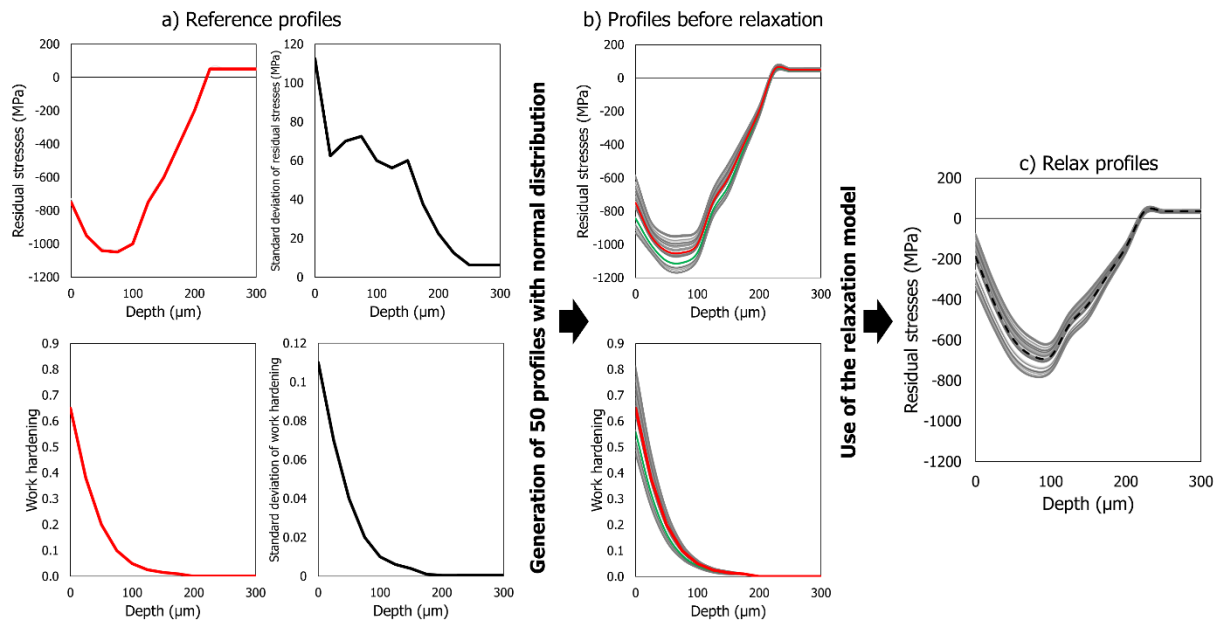
553 i) The part of the results presented in Section 2.3 that have not been used to identify the  
 554 parameters, that is for positions other than  $z_{\sigma_{surf}}$  and  $z_{\sigma_{max}}$ .

555 ii) Additional measurements that have been performed in the framework of the present study  
 556 for the *DA* microstructure and for 50 hours of holding time at 550°C following the protocol detailed  
 557 Section 1.3.

558 iii) Data from Prév y's work [6] which allows the model to be validated under experimental  
 559 conditions not investigated here.

560 For all these data, a statistical analysis has been carried out to consider the experimental scatter and  
 561 the possible errors in the identification of the model. The different steps of this statistical procedure  
 562 are illustrated in Figure 14. With this objective, a pair of initial residual stress and work hardening  
 563 profiles is first generated using a normal distribution with the same randomly chosen probability. The  
 564 initial residual stress and work hardening profiles (solid red lines) have been used as the average values  
 565 of the normal distribution (Figure 14.a). The standard deviation considered in the normal distribution  
 566 is characteristic of the observed experimental scatter. Fifty pairs of initial residual stress and work  
 567 hardening profiles have been generated following this procedure (examples of such profiles are shown  
 568 in green in the Figure 14.b). Then, the model presented in Section 3.2 is applied to all these pairs of  
 569 profiles to obtain 50 profiles of relaxed residual stresses (solid grey lines in the Figure 14.c). The average  
 570 of these profiles is then computed (dashed black line).

571



572

573

574

575

**Figure 14. Steps of the statistical procedure used to validate the model of residual stress relaxation. The red curve represents the reference profiles. The green curves represent an example of a pair of profiles generated with the normal distribution.**

576

577

578

579

580

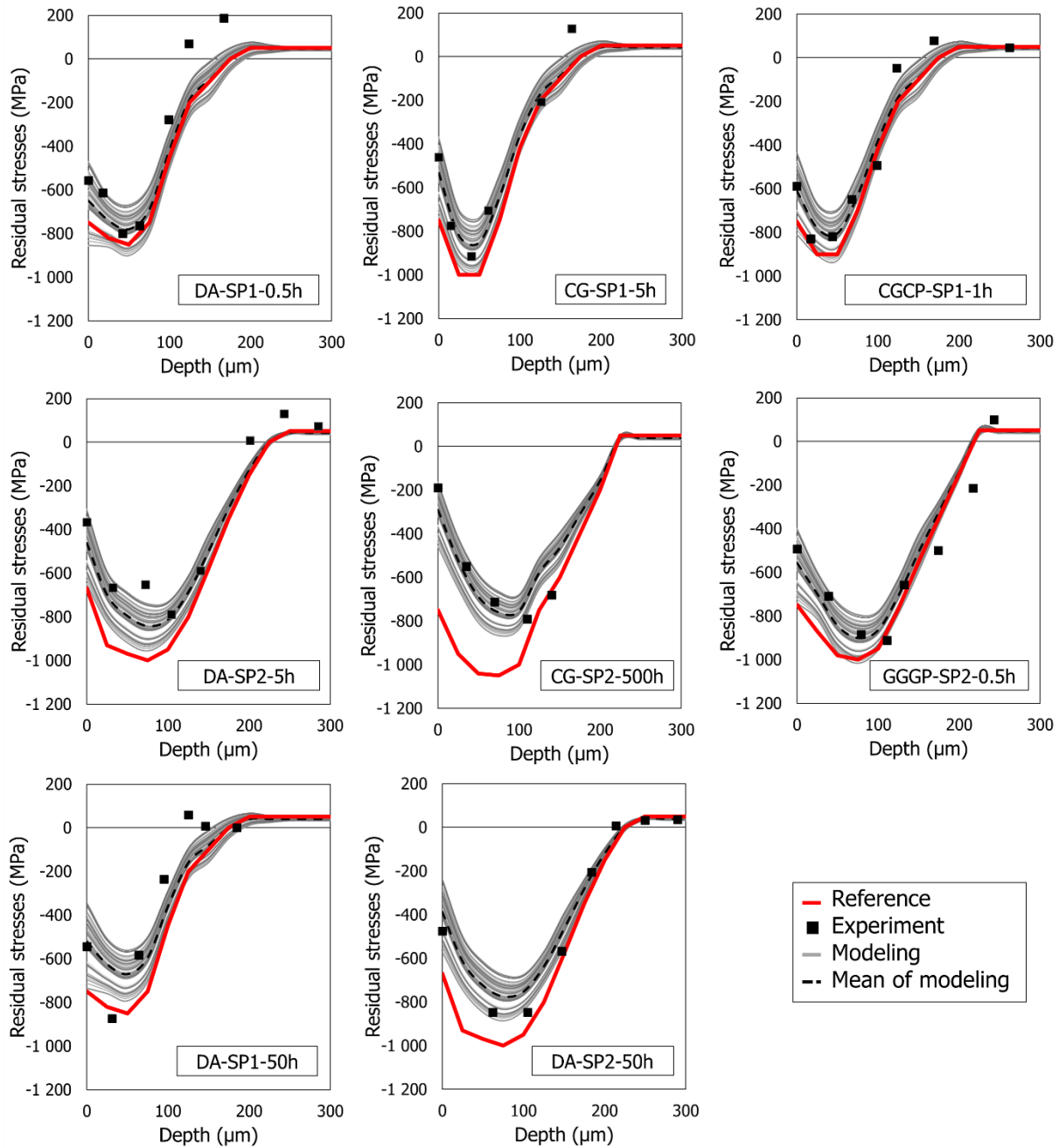
581

582

583

584

This procedure has been first applied to the experimental data obtained in the campaign carried out in this work. The results are presented in Figure 15. For all shot peening conditions and microstructures considered, the average values predicted by the model are in accordance with the experimental data. It is worth noting that the model reproduces particularly well the surface relaxation of the residual stress level, which is strongly influenced by the high level of work hardening. The methodology implemented permits estimation of the relaxation of the residual stresses for the whole depth affected by the process. Additionally, by incorporating experimental dispersion into the procedure, significant variations in residual stress profiles within similar surface treatment and heat treatment conditions can be accurately reflected. These results are consistent with the experimental observations.

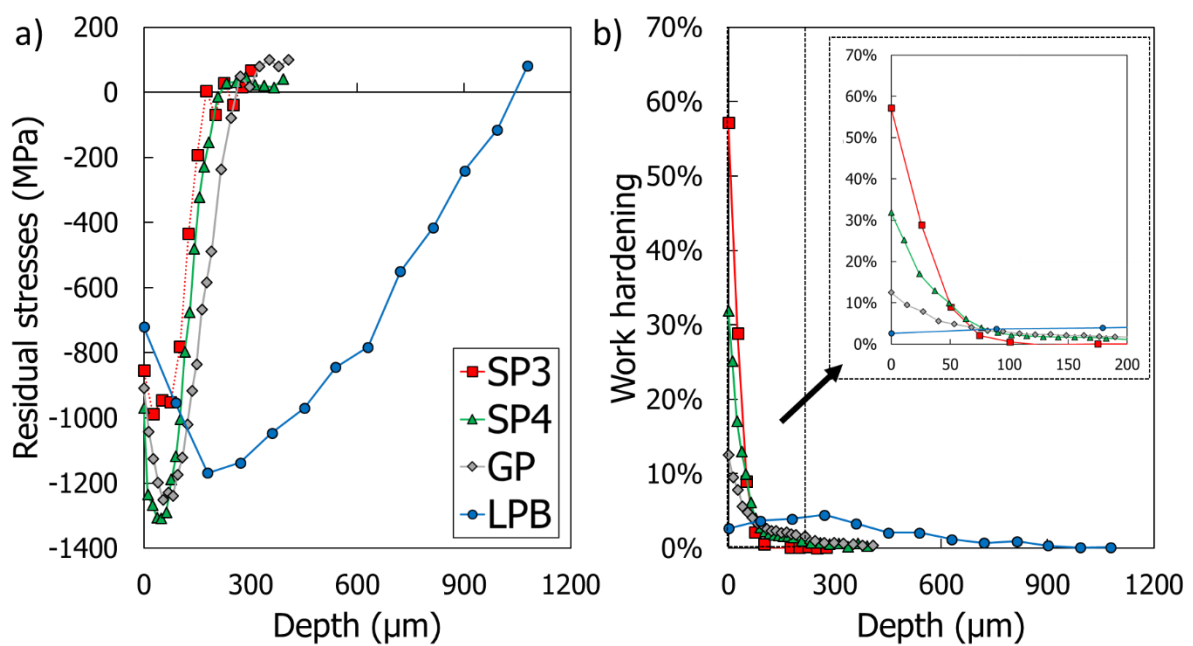


585

586 **Figure 15. Comparison between experimental data and modeling. The labels in the graphs indicate: the**  
 587 **microstructure – the shot peening condition – the holding time.**

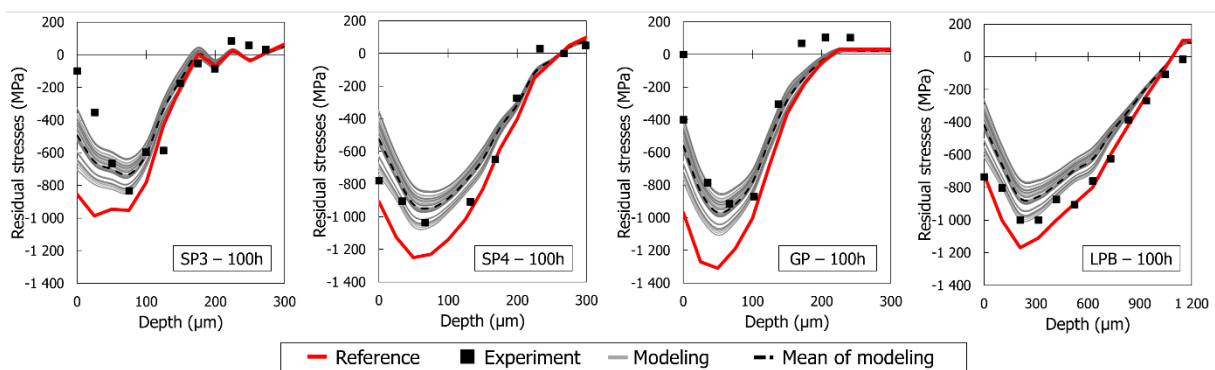
588 The statistical procedure has also been applied to experimental data obtained by Prev y for Inconel  
 589 718 [6]. In Prev y's work, the residual stress and work hardening profiles have been evaluated for  
 590 different surface treatments before and after a heat treatment at 525 C for 100 hours; two shot  
 591 peening conditions (here denoted *SP3* and *SP4*) as well as gravity peening (here noted *GP*) and low  
 592 plastic burnishing (here noted *LPB*) treatments have been studied. Figure 16 presents the initial residual  
 593 stress and work hardening profiles extracted from [6] for the different processes. Note that these four  
 594 surface treatments provide a variety of residual stress and work hardening profiles. The test conditions

595 differ from those of our study (material, measurement conditions, heat treatment temperature); the  
 596 microstructure is not given. These results thus constitute an interesting test for the model proposed in  
 597 Section 3.2. Figure 16 depicts the residual stress relaxation profiles obtained through experimentation  
 598 [6] and the profiles predicted by the model using the statistical analysis outlined above. Once again,  
 599 the model successfully replicates the trends of the experimental results obtained by Prev y. Notably,  
 600 the model accurately estimates the maximum level of residual stress after 100h of holding time at  
 601 525 C. The relaxation of surface residual stresses could be more accurate, as in the previous example  
 602 in Figure 15. However, this analysis confirms the relevance and the pertinence of the proposed  
 603 modeling.



604

605 **Figure 16. Residual stresses (a) and work hardening (b) profiles produced by shot peening (SP3 and SP4),**  
 606 **gravity peening, and low plastic Burnishing in IN718 [6].**



607

608 **Figure 17. Comparison between experiment [6] and modeling of residual stress profiles after 100h holding**  
 609 **time at 525 C.**

## 610 **4 Conclusion**

611 The aim of this work was to establish a model for the influence of work hardening and microstructure  
612 on the evolution of residual stresses under thermal loading. The first step was to analyze the numerous  
613 experimental conditions used in this study to assess the effect of work hardening, grain size and size of  
614 strengthening precipitates on the relaxation of residual stresses. Residual stress and work hardening  
615 profiles were determined on shot peened components for different holding times at 550°C. The  
616 calibration methodology previously proposed [11] allows the influence of different microstructures in  
617 terms of grain size and precipitate size to be evaluated. It has been possible to establish the order of  
618 influence of the parameters on the relaxation of residual stresses under thermal loading. The first order  
619 parameter is work hardening. The higher it is, the greater the relaxation of residual stresses. The second  
620 order parameter is grain size. An increase in this factor leads to a decrease in residual stress relaxation.  
621 Finally, the parameter with the least influence in the study carried out was the size of the strengthening  
622 precipitates, where no clear trend could be deduced from the experimental data analyzed.

623 Based on the experimental results, an analytical model was then proposed which considers the  
624 influence of the work hardening induced by the surface treatment. Several advantages of this model  
625 can be highlighted. The parameters of the model can be identified on the basis of characteristic points  
626 present on the residual stress profiles; at the surface and where the compressive residual stresses are  
627 at their maximum. As a result, only a few points are required to calibrate the model. Once identified, it  
628 can be used to predict the relaxation of residual stresses in depth if the work hardening profile induced  
629 by the surface treatment is known. The proposed model is not limited to the case of shot peening. It  
630 can now be applied to estimate the relaxation of residual stresses on components that may have a  
631 work hardening gradient in the part. As explained in the introduction, shot-peened Inconel 718 parts  
632 are subject to temperature fatigue loading. The study carried out here will therefore make it possible  
633 to decouple the effects of mechanical loading and temperature.

## 634 **5 Acknowledgement**

This work was conducted with the help of the French Technological Research Institute for Materials, Metallurgy and Processes (IRT M2P) under the CONDOR project. The authors would like to acknowledge IRT M2P and all the partners of the project led by IRT M2P. Safran is warmly thanked for its precious collaboration in this work.

## 6 Data availability

The raw/processed data required to reproduce these findings cannot be shared at this time due to legal or ethical reasons.

## 7 References

- [1] M. Benedetti, V. Fontanari, C. Santus, and M. Bandini, "Notch fatigue behaviour of shot peened high-strength aluminium alloys: Experiments and predictions using a critical distance method," *International Journal of Fatigue*, vol. 32, no. 10, pp. 1600–1611, Oct. 2010, doi: 10.1016/j.ijfatigue.2010.02.012.
- [2] Md. S. Bhuiyan, Y. Mutoh, and A. J. McEvily, "The influence of mechanical surface treatments on fatigue behavior of extruded AZ61 magnesium alloy," *Materials Science and Engineering: A*, vol. 549, pp. 69–75, Jul. 2012, doi: 10.1016/j.msea.2012.04.007.
- [3] B. Gerin, E. Pessard, F. Morel, and C. Verdu, "Influence of surface integrity on the fatigue behaviour of a hot-forged and shot-peened C70 steel component," *Materials Science and Engineering: A*, vol. 686, pp. 121–133, 2017, doi: 10.1016/j.msea.2017.01.041.
- [4] T. Klotz, D. Delbergue, P. Bocher, M. Lévesque, and M. Brochu, "Surface characteristics and fatigue behavior of shot peened Inconel 718," *International Journal of Fatigue*, vol. 110, pp. 10–21, May 2018, doi: 10.1016/j.ijfatigue.2018.01.005.
- [5] Z. Qin, B. Li, H. Zhang, T. Youani Andre Wilfried, T. Gao, and H. Xue, "Effects of shot peening with different coverage on surface integrity and fatigue crack growth properties of 7B50-T7751 aluminum alloy," *Engineering Failure Analysis*, vol. 133, p. 106010, Mar. 2022, doi: 10.1016/j.engfailanal.2021.106010.
- [6] P. S. Prevéy, "The Effect of Cold Work on the Thermal Stability of Residual Compression in Surface Enhanced IN718," in *20th ASM Materials Solutions Conference & Exposition*, St. Louis, Missouri, 2000.
- [7] B. Pieraggi and J. F. Uginet, "Fatigue and Creep Properties in Relation with Alloy 718 Microstructure," in *Superalloys 718, 625, 706 and Various Derivatives (1994)*, TMS, 1994, pp. 535–544. doi: 10.7449/1994/Superalloys\_1994\_535\_544.
- [8] W. Chen and M. C. Chaturvedi, "Dependence of creep fracture of Inconel 718 on grain boundary precipitates," *Acta Materialia*, vol. 45, no. 7, pp. 2735–2746, Jul. 1997, doi: 10.1016/S1359-6454(96)00399-0.
- [9] R. E. Schafrik, D. D. Ward, and J. R. Groh, "Application of Alloy 718 in GE Aircraft Engines: Past, Present and Next Five Years," in *Superalloys 718, 625, 706 and Various Derivatives (2001)*, TMS, 2001, pp. 1–11. doi: 10.7449/2001/Superalloys\_2001\_1\_11.
- [10] F. Alexandre, S. Deyber, and A. Pineau, "Modelling the optimum grain size on the low cycle fatigue life of a Ni based superalloy in the presence of two possible crack initiation sites," *Scripta Materialia*, vol. 50, no. 1, pp. 25–30, Jan. 2004, doi: 10.1016/j.scriptamat.2003.09.043.
- [11] J. P. Goulmy *et al.*, "A calibration procedure for the assessment of work hardening part I: Effects of the microstructure and load type," *Materials Characterization*, vol. 175, p. 111067, May 2021, doi: 10.1016/j.matchar.2021.111067.
- [12] J. P. Goulmy *et al.*, "A calibration procedure for the assessment of work hardening Part II: Application to shot peened IN718 parts," *Materials Characterization*, vol. 175, p. 111068, May 2021, doi: 10.1016/j.matchar.2021.111068.
- [13] Surface Integrity, "Tech Report." Manufacturing Engineering, 1989.
- [14] N. Masmoudi Khebou, "Etude de l'évolution des contraintes de grenailage en fatigue à haute température pour le superalliage base nickel IN100," Thèse Doctorat, Arts et Métiers ParisTech, France, 1990.

- [15] I. Lillamand, "Evolution d'une couche grenillée sous sollicitations thermiques et mécaniques, cas de la fatigue oligocyclique," Thèse de doctorat, ENSAM, 1999.
- [16] J. Hoffmeister, V. Schulze, A. Wanner, R. Hessert, and G. Koenig, "Thermal relaxation of residual stresses induced by shot peening in IN718," in *10th International Conference of Shot Peening*, Tokyo, 2008. Accessed: Mar. 12, 2015. [Online]. Available: <http://www.shotpeener.com/library/pdf/2008060.pdf>
- [17] P. S. Prevéy, "The measurement of sub-surface residual stress and cold work distributions in nickel base alloys," in *Residual Stress in Design, Process and Materials Selection*, 1987, pp. 11–19.
- [18] V. Schulze, F. Burgahn, O. Vöhringer, and E. Macherauch, "Zum thermischen Abbau von Kugelstrahl-Eigenspannungen bei vergütetem 42 CrMo 4," *Mat.-wiss. u. Werkstofftech.*, vol. 24, no. 7, pp. 258–267, Jul. 1993, doi: 10.1002/mawe.19930240709.
- [19] J. T. Cammett, P. S. Prevéy, and N. Jayaraman, "The effect of shot peening coverage on residual stress, cold work, and fatigue in a Nickel-Base Superalloy," in *ICSP 9*, Paris, 2005.
- [20] P. Juijerm and I. Altenberger, "Residual stress relaxation of deep-rolled Al–Mg–Si–Cu alloy during cyclic loading at elevated temperatures," *Scripta Materialia*, vol. 55, no. 12, pp. 1111–1114, 2006, doi: 10.1016/j.scriptamat.2006.08.047.
- [21] Z. Zhou *et al.*, "A finite element study of thermal relaxation of residual stress in laser shock peened IN718 superalloy," *International Journal of Impact Engineering*, vol. 38, no. 7, pp. 590–596, Jul. 2011, doi: 10.1016/j.ijimpeng.2011.02.006.
- [22] B. J. Foss, S. Gray, M. C. Hardy, S. Stekovic, D. S. McPhail, and B. A. Shollock, "Analysis of shot-peening and residual stress relaxation in the nickel-based superalloy RR1000," *Acta Materialia*, vol. 61, pp. 2548–2559, 2013.
- [23] O. Vöhringer, "Relaxation of residual stresses by annealing or mechanical treatment," in *Residual Stresses*, A. NIKU-LARI, Ed., Pergamon, 1987, pp. 367–396. Accessed: Mar. 23, 2015. [Online]. Available: <http://www.sciencedirect.com/science/article/pii/B9780080340623500276>
- [24] M.-C. Berger and J. K. Gregory, "Residual stress relaxation in shot peened Timetal 21s," *Materials Science and Engineering: A*, vol. 263, no. 2, pp. 200–204, mai 1999, doi: 10.1016/S0921-5093(98)01165-4.
- [25] B. X. Feng, X. N. Mao, G. J. Yang, L. L. Yu, and X. D. Wu, "Residual stress field and thermal relaxation behavior of shot-peened TC4-DT titanium alloy," *Materials Science and Engineering: A*, vol. 512, no. 1–2, pp. 105–108, juin 2009, doi: 10.1016/j.msea.2009.01.028.
- [26] *Norme AFNOR NFL 06-832*. 1990.
- [27] J. Lu, *Handbook of measurement of residual stresses*. Lilburn, GA, Upper Saddle River, NJ: Fairmont Press ; Distributed by Prentice Hall PTR, 1996.
- [28] M. Kamaya, A. J. Wilkinson, and J. M. Titchmarsh, "Measurement of plastic strain of polycrystalline material by electron backscatter diffraction," *Nuclear Engineering and Design*, vol. 235, pp. 713–725, 2004.
- [29] J. Hoffmeister, V. Schulze, R. Hessert, and G. Koenig, "Effects of the surface treatment on the measured diffraction peak width of Inconel 718," in *ICSP-11*, 2011, pp. 201–206. Accessed: Apr. 11, 2017. [Online]. Available: <http://www.shotpeener.com/library/pdf/2011033.pdf>
- [30] K. A. Soady, B. G. Mellor, G. D. West, G. Harrison, A. Morris, and P. A. S. Reed, "Evaluating surface deformation and near surface strain hardening resulting from shot peening a tempered martensitic steel and application to low cycle fatigue," *International Journal of Fatigue*, vol. 54, pp. 106–117, Sep. 2013, doi: 10.1016/j.ijfatigue.2013.03.019.
- [31] J. P. Goulmy, V. Boyer, D. Retraint, P. Kanoute, L. Tualbi, and E. Rouhaud, "Modeling of the shot peening of a nickel alloy with the consideration of both residual stresses and work hardening," *International Journal of Solids and Structures*, vol. 264, p. 112120, Mar. 2023, doi: 10.1016/j.ijsolstr.2023.112120.
- [32] D. Cai, P. Nie, J. Shan, W. Liu, Y. Gao, and M. Yao, "Precipitation and Residual Stress Relaxation Kinetics in Shot-Peened Inconel 718," *Journal of Materials Engineering and Performance*, vol. 15, no. 5, pp. 614–617, Oct. 2006, doi: 10.1361/105994906X124613.

- [33] R. Fathallah, G. Inglebert, and L. Castex, "Prediction of plastic deformation and residual stresses induced in metallic parts by shot peening," *Materials Science and Technology*, vol. 14, no. 7, pp. 631–639, Jul. 1998, doi: 10.1179/mst.1998.14.7.631.
- [34] A. Atig, R. Ben Sghaier, R. Seddik, and R. Fathallah, "Probabilistic methodology for predicting the dispersion of residual stresses and Almen intensity considering shot peening process uncertainties," *Int J Adv Manuf Technol*, vol. 94, no. 5, pp. 2125–2136, Feb. 2018, doi: 10.1007/s00170-017-1033-3.
- [35] M. Daoud, R. Kubler, A. Bemou, P. Osmond, and A. Polette, "Prediction of residual stress fields after shot-peening of TRIP780 steel with second-order and artificial neural network models based on multi-impact finite element simulations," *Journal of Manufacturing Processes*, vol. 72, pp. 529–543, Dec. 2021, doi: 10.1016/j.jmapro.2021.10.034.
- [36] P. M. M. Sundararaman, "Precipitation of the  $\delta$ -Ni<sub>3</sub>Nb phase in two nickel base superalloys," *Metallurgical and Materials Transactions A-physical Metallurgy and Materials Science - METALL MATER TRANS A*, vol. 19, no. 3, pp. 453–465, 1988, doi: 10.1007/BF02649259.
- [37] P. S. Prév y, D. J. Hornbach, and P. W. Mason, "Thermal Residual Stress Relaxation and Distortion in Surface Enhanced GasTurbine Engine Components," *ASM International*, 1998.
- [38] M. E. Fine, *Introduction to Phase Transformations in Condensed Systems*, First printing. New York: Macmillan, 1964. Accessed: Apr. 19, 2024. [Online]. Available: <https://www.biblio.com/book/introduction-phase-transformations-condensed-systems-fine/d/1298436554>